Disentangling Ligand Effects on Metathesis Catalyst Activity: Experimental and Computational Studies of Ruthenium–Aminophosphine Complexes

Crystal K. Chu, Tzu-Pin Lin, Huiling Shao, Allegra L. Liberman-Martin, Peng Liu, and Robert H. Grubbs

J. Am. Chem. Soc., **Just Accepted Manuscript** • DOI: 10.1021/jacs.8b02324 • Publication Date (Web): 05 Apr 2018

Disentangling Ligand Effects on Metathesis Catalyst Activity: Experimental and Computational Studies of Ruthenium–Aminophosphine Complexes

Crystal K. Chu,† Tzu-Pin Lin,† Huiling Shao,‡ Allegra L. Liberman-Martin,† Peng Liu,*‡ and Robert H. Grubbs*†

†Arnold and Mabel Beckman Laboratories of Chemical Synthesis, California Institute of Technology, Pasadena, California 91125, United States

‡Department of Chemistry, University of Pittsburgh, Pittsburgh, Pennsylvania 15260, United States

ABSTRACT: Second-generation ruthenium olefin metathesis catalysts bearing aminophosphine ligands were investigated with systematic variation of the ligand structure. The rates of phosphine dissociation (k_1; initiation rate) and relative phosphine reassociation (k_{-1}) were determined for two series of catalysts bearing cyclohexyl(morpholino)phosphine and cyclohexyl(piperidino)phosphine ligands. In both cases, incorporating P–N bonds into the architecture of the dissociating phosphine accelerates catalyst initiation relative to the parent [Ru]–PCy_3 complex; however, this effect is muted for the tris(amino)phosphine-ligated complexes, which exhibit higher ligand binding constants in comparison to those with phosphines containing one or two cyclohexyl substituents. These results, along with X-ray crystallographic data and DFT calculations, were used to understand the influence of ligand structure on catalyst activity. Especially noteworthy is the application of phosphines containing incongruent substituents ($PR_1R'_2$); detailed analyses of factors affecting ligand dissociation, including steric effects, inductive effects, and ligand conformation, are presented. Computational studies of the reaction coordinate for ligand dissociation reveal that ligand conformational changes contribute to the rapid dissociation for the fastest-initiating catalyst of these series, which bears a cyclohexyl-bis(morpholino)phosphine ligand. Furthermore, the effect of amine incorporation was examined in the context of ring-opening metathesis polymerization, and reaction rates were found to correlate well with catalyst initiation rates. The combined experimental and computational studies presented in this report reveal important considerations for designing efficient ruthenium olefin metathesis catalysts.

INTRODUCTION

Since its discovery in the 1950s, olefin metathesis has evolved into a versatile and powerful reaction for organic synthesis.[1] Molybdenum, tungsten, and ruthenium catalysts have been extensively investigated in the synthesis of natural and unnatural products, including the formation of substituted olefins and cyclic organic compounds.[2] Furthermore, significant efforts toward the development of olefin metathesis polymerizations,[3] notably ring-opening metathesis polymerization (ROMP)[4] and acyclic diene metathesis (ADMET),[5] have enabled the synthesis of new functional materials[6] and have led to important industrial applications.[7]

Complexes based on molybdenum and tungsten were the earliest reported well-defined olefin metathesis catalysts, and since their initial discovery, have been widely used for their high reactivity.[8] Extensive research of ruthenium-based complexes has resulted in catalysts with increased functional group tolerance and stability to air and moisture. Demonstration of ruthenium alkylidene complexes as viable olefin metathesis catalysts[9] led to the development of catalyst **G1** (Figure 1).[10] The lower activity of **G1** in comparison to molybdenum catalysts was later addressed through the development of second-generation ruthenium olefin metathesis catalysts, notably **G2**,[11] in which a phosphine is substituted for an *N*-heterocyclic carbene (NHC) ligand.[12,13] The bis(pyridine) complex **G3** and related complexes have proven to be fast-initiating, enabling cross metathesis of challenging substrates[14] and ROMP to produce polymers with controlled molecular weight and low dispersity;[15] additionally, complex **G3** can serve as a useful precursor for variants of catalyst **G2** that bear various organic substituents on the phosphine.[16]

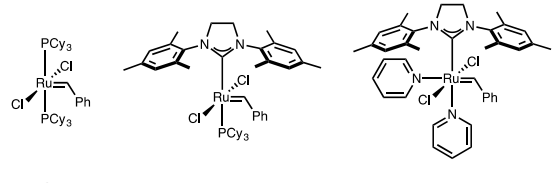

G1 G2 G3

Figure 1. Established ruthenium olefin metathesis catalysts.

Mechanistic studies of olefin metathesis promoted by second-generation ruthenium catalysts have suggested that these reactions occur by a dissociative pathway, in which phosphine dissociation occurs to form a 14-electron intermediate in an initiation step prior to olefin binding (Scheme 1).[17,18] Thus, the activity of these catalysts is affected by the rate of phosphine dissociation (k_1; initiation rate) and the relative rate of phosphine reassociation (k_{-1}).[19] Following formation of the 14-electron intermediate, the likelihood of phosphine reassociation versus productive olefin binding (k_{-1}/k_2) can be experimentally determined; higher binding affinity of the olefin in comparison to the phosphine, rather than differences in initiation kinetics, has been shown to be the underlying cause for the increased metathesis activity of **G2** compared to **G1**.[20]

Scheme 1. Proposed Dissociative Mechanism for Second-Generation Ruthenium Olefin Metathesis Catalysts

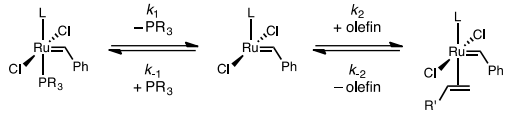

Dissociation rate constants have been reported for a variety of second-generation ruthenium catalysts bearing alkyl- or arylphosphine ligands.[21] Although phosphine electronics are not known to strongly correlate with ligand reassociation, initiation rates have been shown to increase with decreasing σ-donor strength of alkyl- and arylphosphines. With this in mind, we decided to further investigate phosphines with unique σ-donating properties as ligands for metathesis catalysts. Phosphines containing electron-withdrawing substituents, notably halogenated arenes, have been studied; however, the incorporation of P–X bonds, where X is an electronegative heteroatom, has been much less explored in this context. Aminophosphine ligands provide access to a broad range of σ-donating and π-accepting properties[22] of relevance to many catalytic applications.[23,24] NMR studies of aminophosphine adducts have demonstrated decreased σ-basicity of select ligands in comparison to triphenylphosphine.[25] On the other hand, structural studies of *N*-pyrrolidinyl, pyrrolyl, and related phosphines have attributed their electron-rich, basic properties to donation from the nitrogen lone pairs to the lone pair of phosphorus.[26] Drawn to these unique attributes, we became interested in evaluating the influence of aminophosphine ligands in the context of second-generation ruthenium metathesis catalysts. These ligands are particularly well suited to systematically investigate the effect of incorporating P–X bonds on metathesis catalyst activity, quantified herein through rates of initiation, relative phosphine reassociation, and ROMP. The combined experimental and computational results underline the importance of several key factors in promoting phosphine dissociation, providing guidance for the future design of efficient ruthenium olefin metathesis catalysts.

RESULTS AND DISCUSSION

In this study, nitrogen-containing heterocycles were systematically introduced in place of the cyclohexyl groups in complex **G2** to probe the effect of P–N bonds on catalyst activity. NMR spectroscopic and X-ray crystallographic data were obtained to gather structural information, and these data were analyzed in the context of kinetics studies. Initiation rates and the relative phosphine reassociation rates were measured, together providing a metric to compare aminophosphine binding strengths. Trends in ligand binding strengths and initiation rates were investigated using DFT calculations,[27] which account for important parameters affecting ligand properties. Furthermore, the use of phosphines bearing incongruent substituents allows for a more comprehensive understanding of ligand structure, providing additional information regarding the effects of sterics and ligand conformation on phosphine dissociation. Detailed analyses of the kinetics and computational studies, along with the application of the new catalysts in ROMP studies, revealed important factors affecting ligand dissociation energy, initiation rates, and catalyst activity.

Synthesis of Ruthenium Catalysts Featuring Aminophosphine Ligands. Two new series of second-generation ruthenium olefin metathesis catalysts bearing aminophosphine ligands in place of the tricyclohexylphosphine present in catalyst **G2** were synthesized. Morpholine and piperidine substituents were targeted due to their similarity in steric profile to cyclohexane.

Treatment of the appropriate chlorophosphine with excess morpholine or piperidine produced the corresponding aminophosphines **L1–L6** (Scheme 2). Complexations to form catalysts **1–6** were achieved by reacting the bis(pyridine) catalyst **G3** with an excess of the desired aminophosphine in THF.[16]

Scheme 2. Synthesis of Complexes 1–6

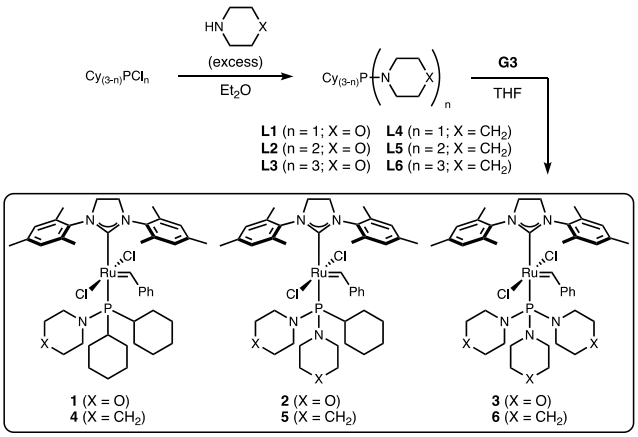

Second-generation ruthenium olefin metathesis catalysts with aromatic phosphine ligands are known to be faster-initiating than their alkylphosphine counterparts,

and the effects of replacing the PCy_3 ligand with PPh_3 in **G2** and related catalysts have been well studied for ring-closing metathesis (RCM)[28] and ROMP[21a] reactions. Thus, following the successful synthesis of catalysts **1–6**, we became interested in potentially faster-initiating species derived from aromatic amines. To this end, a pyrrolylphosphine ligand was synthesized, providing access to complex **7** (Figure 2).

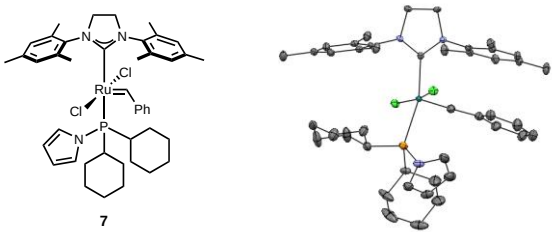

Figure 2. Ruthenium-based olefin metathesis catalyst bearing a pyrrolylphosphine ligand. X-ray crystal structure of **7** with 50% probability ellipsoids (right) and hydrogen atoms omitted for clarity.

Characterization of New Catalysts by NMR Spectroscopy and X-Ray Crystallography. Table 1 lists the ^{31}P NMR chemical shifts for catalysts **G2** and **1–6** along with the corresponding free phosphine ligands. In both the morpholine- and piperidine-based series, the ^{31}P resonance of the free phosphine shifts downfield as amine substitution increases. The same ^{31}P trend is observed in the ruthenium complexes, with the exception of the tris(amino)phosphine complexes **3** (116.9 ppm) and **6** (118.7 ppm), which are more shielded than the bis(amino)phosphine congeners **2** (131.9 ppm) and **5** (133.0 ppm), respectively. Notably, a similar nonlinear trend has been observed in series of aminophosphine complexes of $PdCl_2$ in which the ^{31}P resonance of the tris(amino)phosphine complex is upfield from that of the disubstituted analogue.[29] Collectively, these observations denote intricate steric and electronic effects exerted by these ligands, as evidenced in the crystallographic, kinetic, and computational analyses (*vide infra*).

Table 1. Signature ^{31}P NMR Chemical Shifts[a]

catalyst	cat. (^{31}P)	ligand	free ligand (^{31}P)	Δ ppm
G2	29.4	PCy_3	8.8	20.6
1	92.2	**L1**	75.6	16.6
2	131.9	**L2**	98	33.9
3	116.9	**L3**	114.7	2.2
4	92.1	**L4**	75.9	16.2
5	133.0	**L5**	98.8	34.0
6	118.7	**L6**	116.8	1.9

[a]Measured in benzene-d_6.

To gain structural information, catalysts **4–6**, containing piperidine-substituted phosphine ligands, were selected for further characterization by X-ray crystallography (Figures 3–5). The crystal structures confirm the connectivity expected for these phosphine-ligated complexes. Selected bond lengths and bond angles, including those reported for the parent catalyst **G2**,[21b] are displayed in Table 2 for comparison.

Catalysts **4–6** all have similar Ru–C1 bond lengths when compared to that of the parent catalyst **G2** (Table 2). Additionally, the Ru–P bond of catalyst **4**, with one piperidine substituent, is longer than that of catalyst **5**, which contains two piperidine rings; these Ru–P bond lengths show no direct correlation with rates of phosphine dissociation (*vide infra*). While these analyses reveal no clear trend in the Ru–P and Ru–C1 distances, the Ru–C8 bond lengthens with increasing incorporation of P–N bonds. This observation suggests that the *trans* influence increases in the order of PCy_3 < **L4** < **L5** < **L6**. Furthermore, these complexes crystallize in such a way that one substituent on the phosphine ligand occupies a position below a mesityl ring (NHC) that is oriented away from the benzylidene. For complexes **5** and **6**, a piperidine ring occupies this position (Figures 4 and 5), whereas one of the two cyclohexyl rings takes this position for **G2** and **4** (Figure 3). These structural differences translate to steric and conformational effects important to catalyst reactivity (*vide infra*).

Initiation Kinetics by ^1H NMR Spectroscopy. The effect of P–N bonds on catalyst activity was first analyzed by comparing catalyst initiation rates for **1–6**. The rate constants of phosphine dissociation (k_1) for complexes **G2** and **1–6** were measured at 30 °C in toluene-d_8. These experiments allow for the comparison of two complete series of new morpholinophosphine- (Figure 6) and piperidinophosphine-ligated (Figure 7) catalysts along with the known parent catalyst **G2**. Initiation rate constants of the complexes were determined using a previously described method involving quenching with excess ethyl vinyl ether under pseudo-first-order conditions and monitoring the disappearance of the benzylidene resonance by ^1H NMR spectroscopy.[21a,30]

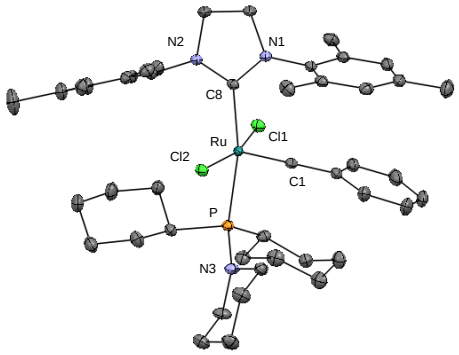

Figure 3. X-ray crystal structure of catalyst **4** with 50% probability ellipsoids. Hydrogen atoms have been omitted for clarity.

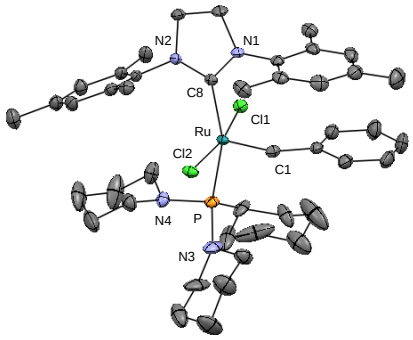

Figure 4. X-ray crystal structure of catalyst **5** with 50% probability ellipsoids. Hydrogen atoms have been omitted for clarity.

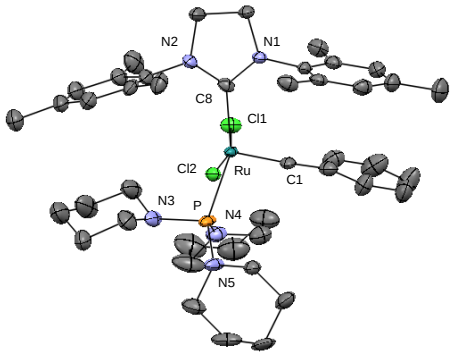

Figure 5. X-ray crystal structure of catalyst **6** with 50% probability ellipsoids. Hydrogen atoms have been omitted for clarity.

Table 2. Selected Bond Lengths (Å) and Bond Angles (º) for Complexes G2 and 4–6.

bond length	**G2**	complex **4**	complex **5**	complex **6**
Ru–C1	1.835(2)	1.836(2)	1.839(3)	1.825(5)
Ru–C8	2.085(2)	2.0877(19)	2.097(3)	2.121(4)
Ru–P	2.4245(5)	2.4340(5)	2.3820(10)	2.394(3)
Ru–Cl1	2.3988(5)	2.4032(5)	2.3944(9)	2.374(5)
Ru–Cl2	2.3912(5)	2.3860(5)	2.4005(10)	2.421(3)
bond angle	**G2**	complex **4**	complex **5**	complex **6**
C1–Ru–C8	100.24(8)	99.70(8)	102.32(14)	102.1(2)
C1–Ru–P	95.89(6)	94.79(6)	100.29(11)	100.64(17)
C8–Ru–P	163.73(6)	165.40(6)	157.29(9)	157.17(14)

Under the same conditions, an experiment to determine the initiation rate of catalyst **7**, bearing a pyrrolylphosphine ligand, resulted in full consumption of the benzylidene faster than the time scale to obtain a precise rate measurement. As expected, catalyst **7** initiates faster than all other complexes reported in this study containing morpholine and piperidine substituents; the lower limit of the initiation rate constant for this catalyst is $> 2 \times 10^{-2}$ s^{-1}. While the reaction kinetics of this complex are not included for the systematic study of amine incorporation, **7** was later tested in ROMP studies (Figure 13).

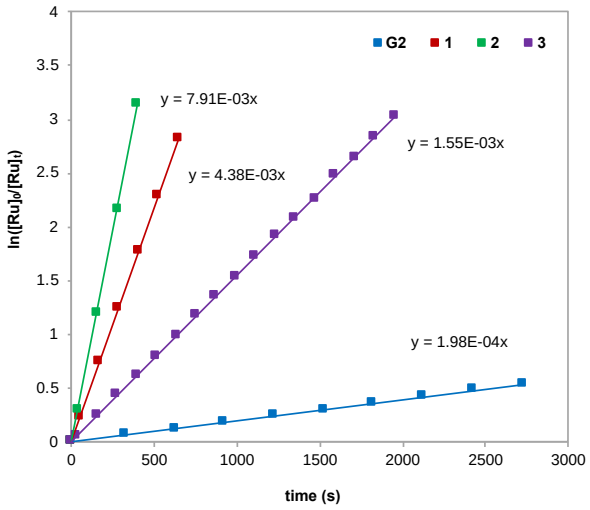

Figure 6. Initiation rates of catalyst series **1–3** bearing morpholinophosphine ligands and catalyst **G2** determined by ^{1}H NMR spectroscopy at 30 °C with $[Ru]_o = 0.017$ M and [ethyl vinyl ether] = 0.5 M (30 equiv.) in toluene-d_8. The rate constants (s^{-1}) of phosphine dissociation are reported as the slopes of the lines fit to pseudo-first-order kinetics.

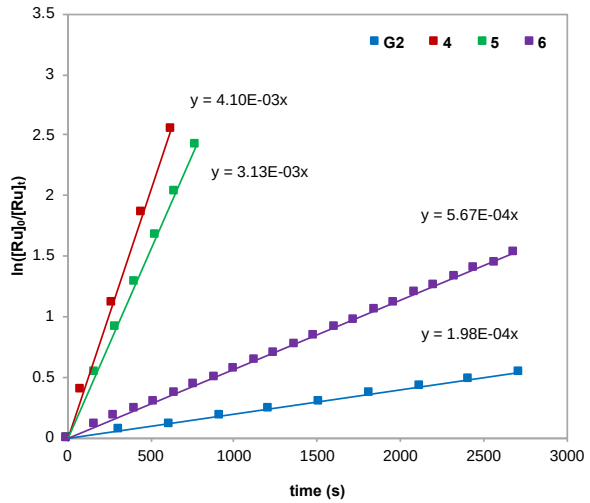

Figure 7. Initiation rates of catalyst series **4–6** bearing piperidinophosphine ligands and catalyst **G2** determined by ^{1}H NMR spectroscopy at 30 °C with $[Ru]_o = 0.017$ M and [ethyl vinyl ether] = 0.5 M (30 equiv.) in toluene-d_8. The rate constants (s^{-1}) of phosphine dissociation are reported as the slopes of the lines fit to pseudo-first-order kinetics.

Table 3. Summary of Initiation Rates for 1–6 and G2.

catalyst	k_i (s^{-1}) at 30 °C	k_{rel} (rel to **G2**)
G2	1.98×10^{-4}	1
1	4.38×10^{-3}	22
2	7.91×10^{-3}	40
3	1.55×10^{-3}	8
4	4.10×10^{-3}	21

5	3.13×10^{-3}	16
6	5.67×10^{-4}	3

In all cases, the aminophosphine ligands dissociate at a faster rate than the PCy_3 ligand of catalyst **G2** (Table 3). In fact, complex **2**, containing a ligand with two morpholine substituents, initiates ~40 times faster than the parent catalyst and has the highest initiation rate of these two series. Interestingly, the tris(amino)phosphine-ligated complexes in both series appear to have anomalous reactivity. While amine substitution seems to dramatically accelerate phosphine dissociation for both mono- and bis(amino)phosphines relative to the PCy_3 ligand of catalyst **G2**, this effect is somewhat muted for the tris(amino)phosphine-ligated complexes **3** and **6**, which are the slowest initiating complexes of each respective series. The initiation rates of catalysts **4–6**, although faster than that of catalyst **G2**, decrease with increasing piperidine substitution (Figure 7). These data suggest that factors other than inductive effects associated with heteroatom incorporation significantly contribute to phosphine donor strength and dissociation rates. Further investigations of catalyst activity, including comparison of phosphine reassociation rates and DFT studies, were required to understand the observed trends in initiation rates.

Determination of k_{-1}/k_2 by ^{1}H NMR Spectroscopy. In order to gain a more complete understanding of the effect of amine substitution on the strength of phosphine binding in second-generation ruthenium catalysts, we next performed experiments to compare the phosphine reassociation rate constants (k_{-1}) at 30 °C in toluene-d_8 by ^{1}H NMR spectroscopy. Following phosphine dissociation, the 14-electron intermediate, which is equivalent for all catalysts discussed in this study, can remain in the catalytic cycle and undergo olefin binding (k_2) or the phosphine can rebind to the metal (k_{-1}). Thus, the measurable ratio k_{-1}/k_2, determined from the slope of the line of best fit according to Equation 1,[31] represents the relative likelihood of these two events. Because phosphine dissociation leads to the same 14-electron intermediate in each case, the propagation rate k_2 is expected to be equivalent for catalysts **G2** and **1–6**. For this reason, studies to determine k_{-1}/k_2 also allow for the comparison of phosphine reassociation rates (k_{-1}) across catalysts **1–6**.

$$\frac{1}{k_{obs}} = \frac{k_{-1}[aminophosphine]}{k_1 k_2 [olefin]} + \frac{1}{k_1} \quad (1)$$

We applied a previously described procedure[21a] for determining relative phosphine reassociation rates to aminophosphine-ligated catalysts, in order to evaluate the effect of P–N bonds on the propensity of these ligands to rebind to the ruthenium center. An example of the results of such an experiment, which incorporates a large excess of ethyl vinyl ether and free phosphine, for catalyst **G2** is shown in Figure 8. The slope of the line of best fit is an estimate for the value of k_{-1}/k_1k_2, and the reciprocal of the y-intercept provides a predicted value of the initiation rate k_1 (Equation 1).

The estimated values of k_{-1}/k_2 for catalysts **G2** and **1–6** are presented in Table 4. For the morpholinophosphine series (**1–3**), the rate of phosphine reassociation directly correlates with amine substitution. As an increasing number of morpholine substituents is systematically introduced into the ligand structure of catalyst **G2**, a gradual increase in k_{-1} is observed. However, this trend is not observed for the piperidinophophine series (**4–6**). Instead, the kinetics of phosphine reassociation are much less varied across this series, and all estimated values of k_{-1} are similar to that of the parent catalyst **G2**.

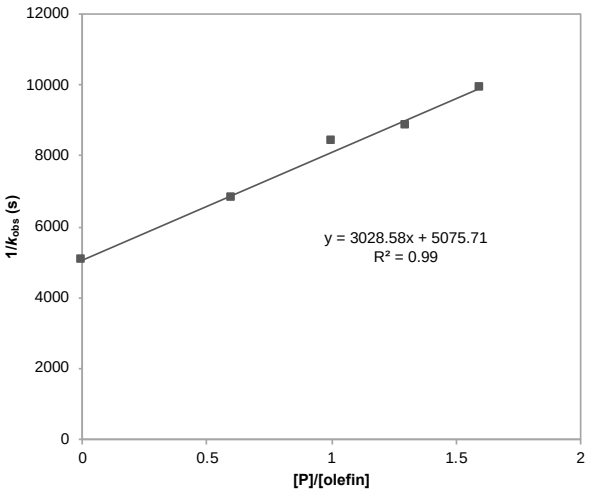

Figure 8. Example plot of $1/k_{obs}$ vs. [P]/[olefin] to measure k_{-1}/k_2 for catalyst **G2** determined by ^{1}H NMR spectroscopy at 30 °C with $[Ru]_0$ = 0.017 M in toluene-d_8.

Furthermore, the measured initiation rates in Table 3 are consistent with predicted values (within 10%) from kinetics experiments performed to compare the relative k_{-1} constants. Along with the linear fitting of $1/k_{obs}$ vs. [P]/[olefin], this observation is consistent with the dissociative mechanism presented in Scheme 1, rather than the associative and interchange mechanisms proposed for other classes of metathesis catalysts.[32]

Observed Trends for Phosphine Binding. The combined results from kinetics studies of complexes **1–6** were analyzed in detail to determine the effect of amine substituents on phosphine binding and to identify key factors that correlate to the observed trends. The relative ratios of k_{-1} to k_1 were calculated for each complex, and

Table 4. Estimated k_{-1}/k_2 Values for Catalysts G2, 1–6.[a]

catalyst	k_{-1}/k_2
G2	0.60
1	1.44
2	1.82
3	3.00

4	0.70
5	0.57
6	0.71

[a]Measured using ^{1}H NMR spectroscopy at 30 °C with $[Ru]_0$ = 0.017 M in toluene-d_8.

this equilibrium constant k_{-1}/k_1, which we will term K_{assoc}, is used as a metric for ligand binding strength. Thus, a more strongly donating ligand is expected to have a higher K_{assoc}, and these values provide an approximation of the relative phosphine binding constants. Normalized values for k_1, k_{-1}, and K_{assoc} are compared across each series **1–3** and **4–6** in Figure 9.

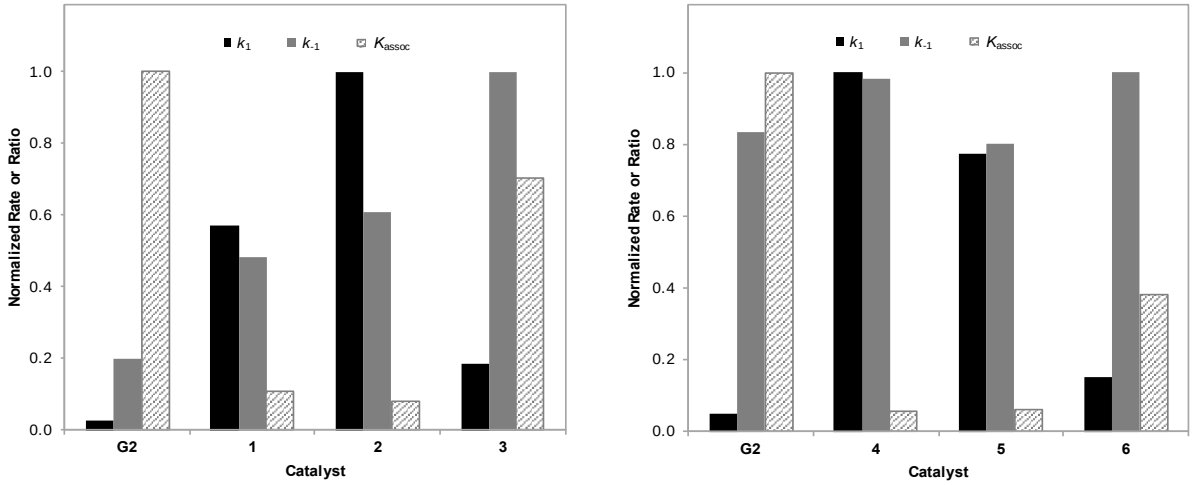

Figure 9. Comparisons of k_1, k_{-1}, and K_{assoc} for catalyst series bearing morpholinophosphine ligands (**1–3**) and piperidinophosphine ligands (**4–6**) as well as catalyst **G2**. All values are normalized with respect to the highest value in each data set (denoted by shading).

shown a related trend in which nucleophilicity increases with the number of amine substituents.[33] As stated previously, the observed trend in k_{-1} for the morpholine series does not hold for the piperidine series. These data suggest that k_{-1} rate constants do not correlate well with inductive effects related to phosphine composition.

The values of K_{assoc} were compared and normalized with respect to that of catalyst **G2**, which has a higher association constant than catalysts **1–6**. Although the trends in phosphine dissociation and reassociation rates in the morpholine series differ from those in the piperidine series, the overall trend in K_{assoc} are the same for both series of aminophosphine-ligated catalysts. For both charts shown in Figure 9, a U-shaped trend is observed for the phosphine association constants as the number of P–N bonds increases from 0 (for catalyst **G2**) to 3 (for catalysts **3** and **6**). While the incorporation of 1 or 2 amine substituents dramatically decreases the binding strength of the phosphine in comparison to **G2**, catalysts **3** and **6** with 3 amine substituents show increased ligand association constants K_{assoc}. Gaining an understanding of the origin of the observed trends in K_{assoc}, and the factors contributing to phosphine dissociation energy, warranted further computational investigations.

Increasing the number of morpholine substituents causes a steady increase in initiation rates when comparing catalysts **G2**, **1**, and **2**. However the tris(morpholino)phosphine ligand breaks this trend, and dissociates at a significantly slower rate. In comparison, the incorporation of piperidine rings into the ligand composition of catalyst **G2** leads to faster-initiating catalysts, but initiation rates decrease as more piperidine substituents are introduced. Despite these differences, the tris(amino)phosphine-ligated complexes **3** and **6** are clearly the slowest-initiating catalysts for both series. Investigations of aminophosphine nucleophilicity have

DFT-Optimized Geometries and Computed Phosphine Dissociation Energies for Morpholinophosphine Catalysts. The morpholine-containing catalysts **1–3** were selected for further computational studies to understand factors affecting phosphine dissociation energies.[34] Catalyst **2**, ligated with cyclohexyl-bis(morpholino)phosphine **L2**, was of special interest since it is the fastest-initiating complex of both series. The structure and conformational flexibility of **L2** were studied by computational methods. Two conformations were identified for the morpholinophosphine ligand, with varied orientation of substituents in relation to the phosphorus lone pair, positioned along the *z*-axis.[35] These low-energy conformations are consistent with the conformation of the PCy_3 ligand in crystal structures.[36] Conformation A, which is less stable in the case of the free ligand, contains a morpholine substituent that is coplanar with the phosphorus *xy*-plane (Figure 10). The ring in this position will be referred to as the "coplanar" substituent. In conformation A, the nitrogen lone pair of the coplanar ring is *anti*-periplanar to the phosphorus lone pair. Previous spectroscopic studies of aminophosphines have suggested that one nitrogen lone pair must take an unprivileged orientation, resulting in a repulsive, pseudo-π interaction

with the phosphorus lone pair.[37] The lone pair–lone pair repulsive interaction results in conformation A being the less stable conformer. Furthermore, the orthogonal cyclohexyl ring present in this ligand conformation exhibits significant steric clash with both morpholine rings. In comparison, conformation B contains two orthogonal morpholine rings and a coplanar cyclohexyl ring with respect to the phosphorus *xy*-plane, and is the favored conformation for the free phosphine.

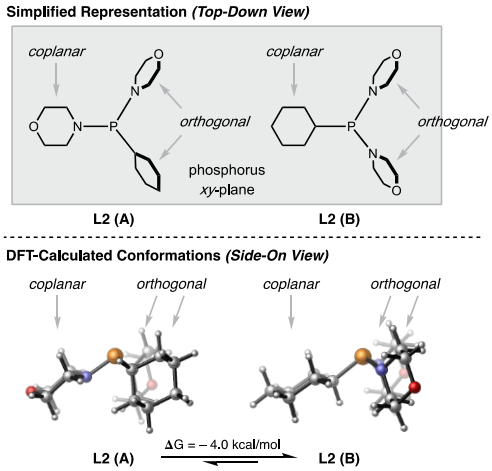

Figure 10. Two perspectives of conformations A and B of ligand **L2** and the computed relative energies. All energies were calculated using the M06/def2TZVP/SMD(toluene)//M06/def2SVP level of theory.

In order to provide insight into the origin of the relative aminophosphine association constants, K_{assoc}, shown in Figure 9, the DFT-optimized geometries (Figure 11) as well as the Gibbs free energies (ΔG_d) and enthalpies (ΔH_d) of phosphine dissociation (Table 5), were computed for parent catalyst **G2** and complexes **1–3**. The calculated ΔG_d and ΔH_d values agree with the U-shaped trend from experimentally determined K_{assoc}; lower phosphine dissociation energies were calculated for complexes **1** and **2** in comparison to **G2** and **3**. The optimized catalyst structures depict variations in ligand conformation and steric repulsions between the coplanar phosphine substituent and the NHC mesityl group. We surmised that the U-shaped trend in phosphine dissociation energy is the combined result of these factors as well as inductive effects derived from increased heteroatom incorporation. Therefore, we conducted a detailed computational analysis of the contributions of these individual factors.

The parent complex **G2**, bearing a PCy_3 ligand, displays an unfavorable steric interaction between the NHC mesityl and the coplanar cyclohexyl ring (Figure 11). Similarly, in complex **1**, a coplanar cyclohexyl ring is oriented toward the *N*-mesityl, a conformation that is corroborated by the crystal structure of the analogous monopiperidinophosphine-ligated complex **4** (Figure 3). These steric clashes between the *P*-cyclohexyl and *N*-mesityl promote phosphine dissociation from catalysts **G2** and **1**; the lower ΔG_d of **1** can be attributed to the inductive effect of the morpholine substituent leading to lower phosphine donor strength. In contrast, the optimized structures of complexes **2** and **3** both contain a coplanar morpholine ring oriented toward the *N*-mesityl; similar structural characteristics are confirmed in the crystal structures of the analogous complexes in the piperidine series **5** and **6** (Figures 4 and 5). The decreased pyramidalization of the morpholine nitrogen atom compared to the cyclohexyl carbon leads to smaller phosphine-NHC repulsions in **2** and **3** compared to the repulsions observed in **G2** and **1** (Figure 11).

Distortion of the aminophosphine ligand is another factor that promotes phosphine dissociation. The computed ligand distortion energies ($\Delta E_{distort}$) in complexes **G2** and **1–3** clearly indicate more significant distortion of ligand **L2** in complex **2** compared to those of the other phosphine ligands (Table 5). The enhanced distortion of **L2** is due to a conformational change upon binding to the ruthenium center. In comparison to the free ligand, the metal-bound ligand **L2** adopts a higher energy conformation with a coplanar morpholine ring (Conformation A, Figure 10) to minimize steric clashes with the NHC mesityl group. Thus, while it does not exhibit the phosphine-NHC steric interactions that promote phosphine dissociation in complexes **G2** and **1**, complex **2** has a low ΔG_d due to a significant contribution from ligand distortion energy.

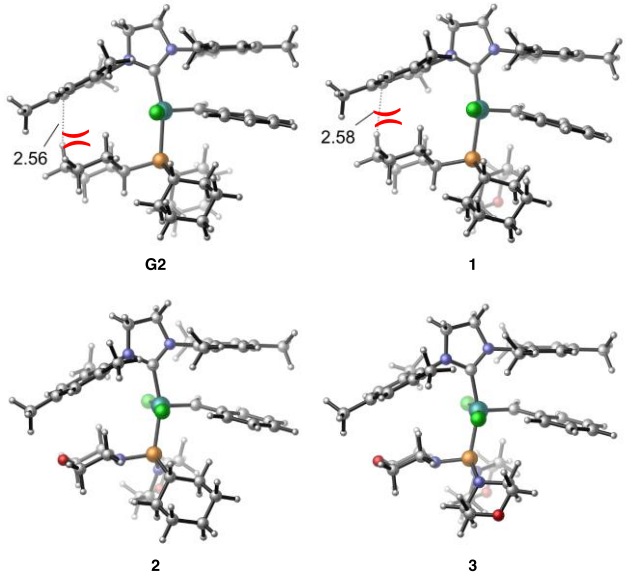

Figure 11. DFT-optimized structures for complexes **G2** and **1–3** depicting steric repulsions between the *N*-mesityl and *P*-cyclohexyl groups in **G2** and **1** and the preferred ligand conformations in **1** and **2**.

While dissociation of ligands with more cyclohexyl substituents (*e.g.* **G2** and **1**) is promoted by steric interactions, the dissociation of ligands with more morpholine substituents (*e.g.* **2** and **3**) is promoted by

Table 5. Calculated Phosphine Ligand Dissociation (ΔG_d, ΔH_d) and Distortion ($\Delta E_{distort}$) Energies.

catalyst	ΔG_d (kcal/mol)[a]	ΔH_d (kcal/mol)[a]	$\Delta E_{distort}$ (kcal/mol)[b]	Promoters of Ligand Dissociation[c]
G2	12.6	30.3	2.9	Steric
1	9.9	27.8	2.7	Steric, Inductive
2	9.5	27.6	5.7	Inductive, Distortion
3	11.9	29.2	1.9	Inductive

All energies were calculated using the M06/def2TZVP/SMD(toluene)//M06/def2SVP level of theory. [a]Ligand dissociation energies ΔG_d and ΔH_d are defined as the Gibbs free energy and enthalpy differences, respectively, between the optimized catalyst and the 14-electron complex plus the free phosphine. [b]Ligand distortion energy ($\Delta E_{distort}$) is defined as the energy difference between the metal-bound phosphine ligand geometry and the optimized free ligand geometry. [c]"Steric" refers to steric repulsions between the coplanar cyclohexyl ring on the phosphine ligand and the NHC mesityl group. "Inductive" describes the inductive effect arising from electron-withdrawing morpholine substituents. "Distortion" refers to distortion of the phosphine ligand in the catalyst.

inductive effects of the nitrogen atoms, which decrease the donor ability of the phosphorus lone pair. This electronic effect is corroborated by the computed Tolman Electronic Parameter (TEP) values for PCy_3 and **L1–L3** (Table 6).[38] As expected, morpholine substitution increases TEP values within a single ligand conformation, indicating decreased phosphine donor strength. For ligands **L1** and **L2**, two different conformations, which contain either a coplanar morpholine (A) or a coplanar cyclohexyl group (B) were individually considered. In these cases, conformation A, which features *anti*-periplanar geometry of the nitrogen and phosphorus lone pairs, exhibits higher phosphine donor strength than conformation B.[37] Thus, the donor ability of the phosphine ligand is dependent on both inductive effects and the preferred ligand conformation in the catalyst. The lowest energy phosphine ligand conformations in complexes **1** and **2**, **L1(B)** and **L2(A)**, have similar TEP values (2064.3 cm^{-1} and 2063.5 cm^{-1}, respectively), suggesting that these two ligands have similar donor strength. Nonetheless, the phosphine donor strength alone cannot explain the dissociation energy trend. While complex **3** exhibits the strongest inductive effects expected to promote phosphine dissociation, a relatively high ΔG_d is observed, indicating the significant contributions of other factors, notably steric interactions and ligand distortion, in promoting ligand dissociation.

The computational analysis revealed that the combined contributions from steric interactions, inductive effects, and ligand distortion result in the U-shaped trends in K_{assoc} and ΔG_d. Accounting for the key promoters of ligand dissociation for each complex, listed in Table 5, provides an explanation for this trend. Ligand dissociation is promoted in **G2** and **1** by phosphine-NHC steric repulsions, and ΔG_d is further reduced in **1** due to inductive effects of the morpholine substituent. Dissociation from complex **2** is promoted by inductive effects and greater distortion of the phosphine ligand. The dissociation from complex **3** is promoted by increased inductive effects; however, significant contributions from phosphine-NHC steric interactions and ligand distortion are not observed to promote the dissociation of **L3**.

Table 6. Calculated Tolman Electronic Parameter (TEP) Values[a] of Phosphine Ligands.

	Conformation A[b]	**Conformation B[b]**
ligand	TEP (cm^{-1})	TEP (cm^{-1})
PCy_3	---	**2060.0**
L1	2058.5	**2064.3**
L2	**2063.5**	2068.3
L3	**2068.3**	---

[a]Vibrational frequencies computed with B3LYP/6-31G(d)-LANL2DZ in the gas phase in $Ni(CO)_3L$; computed frequencies are scaled with a scaling factor of 0.962. [b]In each case, conformation A contains a morpholine ring coplanar to the phosphorus *xy*-plane, whereas conformation B features a coplanar cyclohexyl ring, analogous to the structures in Figure 10. TEP values that correspond to the preferred phosphine conformations in complexes **G2** and **1–3** are highlighted in bold.

Modeling of the Reaction Coordinate of Ligand Dissociation for Fast-Initiating Catalyst 2. Computational studies of the reaction coordinate for phosphine ligand dissociation according to the mechanism in Scheme 1 were performed to determine the origin of the high initiation rate for catalyst **2**, and the reason for faster phosphine dissociation for **2** in comparison to **1**. The reaction coordinate diagrams for the dissociation of catalysts **1** and **2** are shown in Figure 12. While ligand **L1** in catalyst **1** maintains the same conformation (B) throughout the dissociation process, **L2** undergoes a conformational change after the Ru–P distance is elongated to greater than 3.0 Å. As discussed above, in the ground state of catalyst **2**, **L2** adopts the more distorted conformation A ($\Delta E_{distort}$ = 5.7 kcal/mol) to minimize phosphine-NHC steric repulsions. As the Ru–P bond lengthens during phosphine dissociation, the phosphine-NHC repulsion diminishes, and thus the less distorted conformation B becomes more favorable. Although location of the phosphine dissociation transition states was not successful, the computed reaction coordinate diagrams suggest that the dissociation of **L2** is kinetically more favorable than that of **L1** due to the adoption of a lower energy conformation of **L2** in the transition state region. Therefore, the stabilizing effect resulting from this conformational change from A to B is proposed to be the reason that catalyst **2** has a higher rate of phosphine dissociation (k_1) than **1** and is the fastest-initiating catalyst in the series.

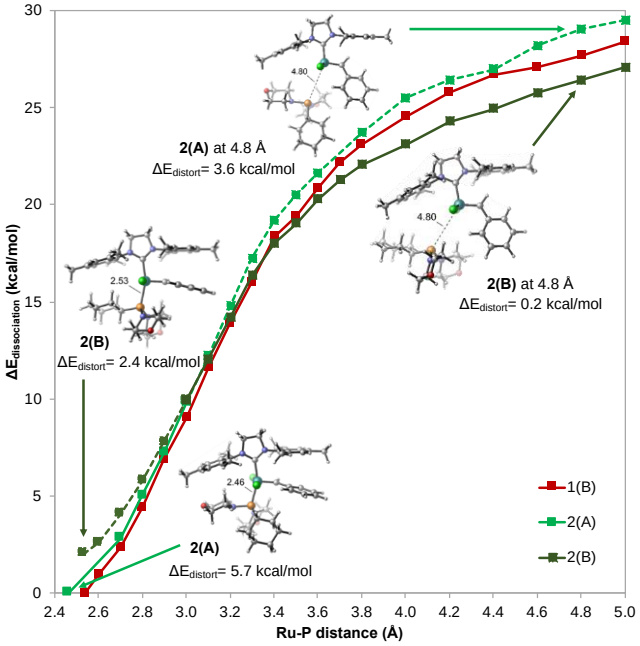

Figure 12. Reaction coordinate diagrams of phosphine ligand dissociation for catalysts **1** and **2**. The corresponding ligand conformation is designated in parentheses (see Figure 10). Both conformations A (more distorted with a coplanar morpholine ring) and B (less distorted with a coplanar cyclohexyl ring) are considered for catalyst **2**. The lowest-energy dissociation pathway of catalyst **2** follows the solid line, starting from conformation A and continuing on to conformation B at longer Ru–P distances. All energies were calculated using the M06/SDD-6-311+G(d,p)/SMD(toluene)//B3LYP/SDD-6-31G(d) level of theory.

Ring-Opening Metathesis Polymerizations. In order to investigate the catalytic activity of the new complexes, they were next evaluated in ROMP, and the reaction kinetics as well as dispersities of the resulting polymers were compared. The substituted norbornene **8** was selected as a model monomer[39] to distinguish the catalytic activities of piperidinophosphine-ligated complexes **4**–**6** from those of catalysts **G2** and **G3**, and to identify potential correlations with the previously determined rate constants (Figure 13). Catalyst **G3** is known to be an efficient and effective ROMP catalyst, while use of the parent catalyst **G2** can lead to uncontrolled molecular weights and broad molecular weight distributions.[15] Furthermore, the activity of the fast-initiating catalyst **7** containing a pyrrole substituent was evaluated.

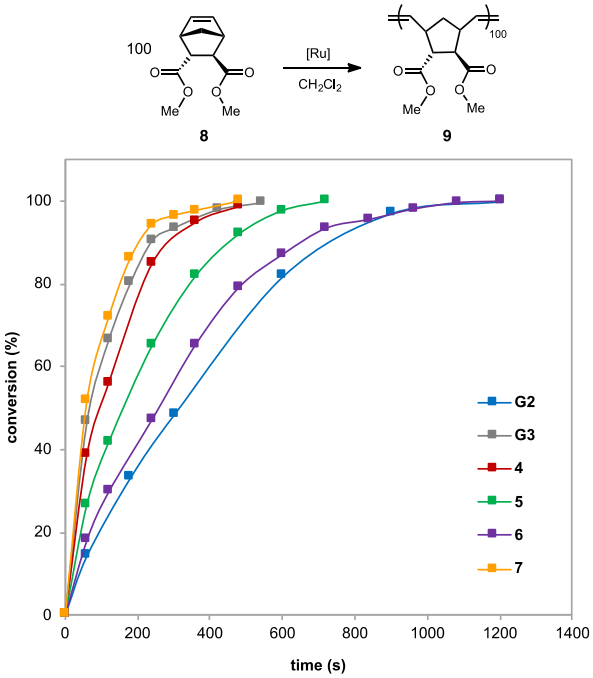

Figure 13. ROMP reaction profiles of aminophosphine-ligated complexes **4**–**7** compared to known catalysts **G2** and **G3**.

The ROMP of **8** was performed in DCM at 25 ºC and monomer conversion was monitored by size-exclusion chromatography (SEC) and ^{1}H NMR spectroscopy. All tested aminophosphine-ligated complexes had higher rates of polymerization than the parent catalyst **G2**, which showed the lowest rate of conversion and broadest molecular weight distribution. For the piperidine catalyst series **4**–**6**, rates of polymerization directly correlate with initiation rates; while amine substitution causes an increase in reactivity relative to **G2**, the rate of polymerization decreases as the number of P–N bonds (*n*) increases, provided $n > 0$. The dispersities of the resulting polymers follow a similar trend, with catalyst **4** providing a narrower molecular weight distribution in comparison to **6**. Furthermore, although none of the catalysts in this series prove to be as efficient as **G3** in the ROMP of **8**, polymerization with the fast-initiating pyrrolylphosphine-ligated catalyst **7** proceeded with a rate of conversion slightly higher than that of **G3**, with similarly low dispersity (1.03). Through the utilization of aminophosphine ligands, a simple change to a substituent in the phosphine ligand of **G2** results in the formation of much more efficient ROMP catalysts with reaction kinetics comparable to **G3**.

CONCLUSIONS

A new class of olefin metathesis catalysts, based on the incorporation of P–N bonds in the phosphine ligand architecture of second-generation ruthenium catalyst **G2**, was synthesized. Following facile synthesis of the aminophosphine ligands from morpholine and piperidine, the catalysts were formed in one step from complex **G3**. The initiation rate and relative phosphine reassociation

rate constants were determined, allowing for the comparison of aminophosphine ligand binding strengths. The results of kinetics and computational studies reveal that a combination of steric, inductive, and ligand conformational effects contribute to the observed trends in phosphine dissociation. Furthermore, DFT calculations suggest that a ligand conformational change during phosphine dissociation is responsible for the accelerated initiation rate of catalyst **2**. Finally, the application of aminophosphine-ligated catalysts to ROMP demonstrates that simple changes to the substituents on the phosphine ligand can lead to a dramatic enhancement in catalyst reactivity. This study unambiguously disentangles the steric, electronic, and conformational effects of aminophosphine ligands on ruthenium metathesis catalyst activity. Investigations of novel phosphine classes, notably those containing incongruent substituents and P–X bonds, will facilitate catalyst design and accelerate the development of efficient, fast-initiating metathesis catalysts.

ASSOCIATED CONTENT

Supporting Information

Experimental procedures, spectroscopic data, crystallographic data, CIFs of catalysts **4–7**, computational methods, and optimized Cartesian coordinates and energies. This material is available free of charge via the Internet at http://pubs.acs.org.

AUTHOR INFORMATION

Corresponding Authors

* pengliu@pitt.edu
* rhg@caltech.edu

Notes

The authors declare no competing financial interest.

ACKNOWLEDGMENT

We thank Dr. David VanderVelde for assistance with NMR spectroscopic experiments and Lawrence Henling for assistance with X-ray crystallography. Dr. Mona Shahgholi and Naseem Torian are acknowledged for assistance with mass spectrometry. Dr. Adam Johns is thanked for helpful discussions regarding aminophosphine and catalyst synthesis. Dr. Choon Woo Lee, Dr. Keary Engle, Dr. William Wolf, Lennon Luo, and Tonia Ahmed are acknowledged for helpful discussions of kinetics of olefin metathesis. Materia, Inc. is thanked for donation of catalyst **G2**. We acknowledge ONR (N00014-13-1-0895 and N00014-14-1-0650) and ARPA-E (DE-AR0000683) for financial support, and the Resnick Sustainability Institute for a fellowship to A.L.L.-M. DFT calculations were performed at the Center for Research Computing at the University of Pittsburgh and the Extreme Science and Engineering Discovery Environment (XSEDE) supported by the National Science Foundation.

REFERENCES

1. For reviews, see: (a) Trnka, T. M.; Grubbs, R. H. *Acc. Chem. Res.* **2001,** *34*, 18–29. (b) Connon, S. J.; Blechert, S. *Angew. Chem., Int. Ed.* **2003,** *42*, 1900–1923. (c) Schrock, R. R.; Hoveyda, A. H. *Angew. Chem., Int. Ed.* **2003,** *42*, 4592–4633. (d) Grubbs, R. H. *Tetrahedron* **2004,** *60*, 7117–7140. (e) Hoveyda, A. H.; Zhugralin, A. R. *Nature* **2007,** *450*, 243–251. (f) Hoveyda, A. H. *J. Org. Chem.* **2014,** *79*, 4763–4792.

2. For reviews, see: (a) Fürstner, A. *Angew. Chem., Int. Ed.* **2000,** *39*, 3012–3043. (b) Monfette, S.; Fogg, D. E. *Chem. Rev.* **2009,** *109*, 3783–3816.

3. For reviews, see: (a) Buchmeiser, M. R. *Chem. Rev.* **2000,** *100*, 1565–1604. (b) Knall, A.-C.; Slugovc, C. In *Olefin Metathesis: Theory and Practice*; Grela, K., Ed.; John Wiley & Sons, Inc.: Hoboken, NJ, 2014; pp 269–284.

4. For reviews of ROMP, see: (a) Bielawski, C. W.; Grubbs, R. H. *Prog. Polym. Sci.* **2007,** *32*, 1–29. (b) Leitgeb, A.; Wappel, J.; Slugovc, C. *Polymer* **2010,** *51*, 2927–2946. (c) Schrock, R. R. *Acc. Chem. Res.* **2014,** *47*, 2457–2466.

5. For a review of ADMET, see: Atallah, P.; Wagener, K. B.; Schulz, M. D. *Macromolecules* **2013,** *46*, 4735–4741.

6. Sutthasupa, S.; Shiotsuki, M.; Sanda, F. *Polym. J.* **2010,** *42*, 905–915.

7. For reviews of olefin metathesis in industry, see: (a) Mol, J. C. *J. Mol. Catal. A: Chem.* **2004,** *213*, 39–45. (b) Slugovc, C. In *Olefin Metathesis: Theory and Practice*; Grela, K., Ed.; John Wiley & Sons, Inc.: Hoboken, NJ, 2014; pp 329–333.

8. (a) Schrock, R. R.; Feldman, J.; Cannizzo, L. F.; Grubbs, R. H. *Macromolecules* **1987,** *20*, 1169–1172. (b) Murdzek, J. S.; Schrock, R. R. *Organometallics* **1987**, *6*, 1373–1374. (c) Schrock, R. R.; DePue, R. T.; Feldman, J.; Schaverien, C. J.; Dewan, J. C.; Liu, A. H. *J. Am. Chem. Soc.* **1988**, *110*, 1423–1435. (d) Bazan, G. C.; Khosravi, E.; Schrock, R. R.; Feast, W. J.; Gibson, V. C.; O'Regan, M. B.; Thomas, J. K.; Davis, W. M. *J. Am. Chem. Soc.* **1990,** *112*, 8378–8387. (e) Schrock, R. R.; Murdzek, J. S.; Bazan, G. C.; Robbins, J.; DiMare, M.; O'Regan, M. *J. Am. Chem. Soc.* **1990**, *112*, 3875–3886.

9. (a) Nguyen, S. T.; Johnson, L. K.; Grubbs, R. H.; Ziller, J. W. *J. Am. Chem. Soc.* **1992,** *114*, 3974–3975. (b) Nguyen, S. T.; Grubbs, R. H.; Ziller, J. W. *J. Am. Chem. Soc.* **1993,** *115*, 9858–9859.

10. Schwab, P.; Grubbs, R. H.; Ziller, J. W. *J. Am. Chem. Soc.* **1996,** *118*, 100–110.

11. Scholl, M.; Ding, S.; Lee, C. W.; Grubbs, R. H. *Org. Lett.* **1999,** *1*, 953–956.

12. For reviews of ruthenium catalysts containing NHC ligands, see: (a) Samojłowicz, C.; Bieniek, M.; Grela, K. *Chem. Rev.* **2009,** *109*, 3708–3742. (b) Vougioukalakis, G. C.; Grubbs, R. H. *Chem. Rev.* **2010,** *110*, 1746–1787.

13. Getty, K.; Delgado-Jaime, M. U.; Kennepohl, P. *J. Am. Chem. Soc.* **2007,** *129*, 15774–15776.

14. Love, J. A.; Morgan, J. P.; Trnka, T. M.; Grubbs, R. H. *Angew. Chem., Int. Ed.* **2002,** *41*, 4035–4037.

15. Choi, T.-L.; Grubbs, R. H. *Angew. Chem., Int. Ed.* **2003,** *42*, 1743–1746.

16. Sanford, M. S.; Love, J. A.; Grubbs, R. H. *Organometallics* **2001,** *20*, 5314–5318.

17. (a) van der EideEdwin, F.; Piers, W. E. *Nat. Chem.* **2010,** *2*, 571–576. (b) Nelson, D. J.; Manzini, S.; Urbina-Blanco, C. A.; Nolan, S. P. *Chem. Commun.* **2014,** *50*, 10355–10375.

18. For computational studies of the dissociative pathway for second-generation ruthenium catalysts, see: (a) Vyboishchikov, S. F.; Bühl, M.; Thiel, W. *Chem. Eur. J.* **2002**, *8*, 3962–3975. (b) Cavallo, L. *J. Am. Chem. Soc.* **2002**, *124*, 8965–8973. (c) Adlhart, C.; Chen, P. *J. Am. Chem. Soc.* **2004**, *126*, 3496–3510. (d) Minenkov, Y.; Occhipinti, G.; Heyndrickx, W.; Jensen, V. R. *Eur. J. Inorg. Chem.* **2012**, *2012*, 1507–1516.

19. Griffiths, J. R.; Diver, S. T. In *Handbook of Metathesis*; Grubbs, R. H., Wenzel, A. G., O'Leary, D. J., Khosravi, E., Eds.; Wiley-VCH: Weinheim, Germay, 2015; pp 273–303.

20. Sanford, M. S.; Ulman, M.; Grubbs, R. H. *J. Am. Chem. Soc.* **2001,** *123*, 749–750.

21. (a) Sanford, M. S.; Love, J. A.; Grubbs, R. H. *J. Am. Chem. Soc.* **2001,** *123*, 6543–6554. (b) Love, J. A.; Sanford, M. S.; Day, M. W.; Grubbs, R. H. *J. Am. Chem. Soc.* **2003,** *125*, 10103–10109.
22. Moloy, K. G.; Petersen, J. L. *J. Am. Chem. Soc.* **1995,** *117*, 7696–7710.
23. For a review of aminophosphine chemistry, see: Gopalakrishnan, J. *Appl. Organomet. Chem.* **2009,** *23*, 291–318.
24. For applications of aminophosphine ligands in catalysis, see: (a) Urgaonkar, S.; Nagarajan, M.; Verkade, J. G. *Tetrahedron Lett.* **2002,** *43*, 8921–8924. (b) Urgaonkar, S.; Nagarajan, M.; Verkade, J. G. *Org. Lett.* **2003,** *5*, 815–818. (c) Tang, H.; Menzel, K.; Fu, G. C. *Angew. Chem., Int. Ed.* **2003,** *42*, 5079–5082. (d) Oberholzer, M.; Frech, C. M. *Green Chem.* **2013,** *15*, 1678–1686. (e) Kitano, T.; Komuro, T.; Ono, R.; Tobita, H. *Organometallics* **2017**, *36*, 2710–2713.
25. (a) Kroshefsky, R. D.; Weiss, R.; Verkade, J. G. *Inorg. Chem.* **1979,** *18*, 469–472. (b) Barnard, T. S.; Mason, M. R. *Inorg. Chem.* **2001,** *40*, 5001–5009. (c) Dyer, P. W.; Fawcett, J.; Hanton, M. J.; Kemmitt, R. D. W.; Padda, R.; Singh, N. *Dalton Trans.* **2003**, 104–113.
26. (a) Clarke, M. L.; Cole-Hamilton, D. J.; Slawin, A. M. Z.; Woollins, J. D. *Chem. Commun.* **2000**, 2065–2066. (b) Clarke, M. L.; Holliday, G. L.; Slawin, A. M. Z.; Woollins, J. D. *J. Chem. Soc., Dalton Trans.* **2002**, 1093–1103.
27. For overviews of computational studies related to ruthenium olefin metathesis catalysts, see: (a) Credendino, R.; Poater, A.; Ragone, F.; Cavallo, L. *Catal. Sci. Technol.* **2011**, *1*, 1287–1297. (b) Liu, P.; Taylor, B. L. H.; Garcia-Lopez, J.; Houk, K. N., In *Handbook of Metathesis*; Grubbs, R. H., Wenzel, A. G., O'Leary, D. J., Khosravi, E., Eds.; Wiley-VCH: Weinheim, Germay, 2015; pp 199–252.
28. Huang, J.; Stevens, E. D.; Nolan, S. P.; Petersen, J. L. *J. Am. Chem. Soc.* **1999,** *121*, 2674–2678.
29. Bolliger, J. L.; Frech, C. M. *Chem. Eur. J.* **2010,** *16*, 4075–4081.
30. Maynard, H. D.; Okada, S. Y.; Grubbs, R. H. *Macromolecules* **2000,** *33*, 6239–6248.
31. See Ref. 21(a) for a derivation of Equation 1.
32. (a) Vorfalt, T.; Wannowius, K.-J.; Plenio, H. *Angew. Chem., Int. Ed.* **2010**, *49*, 5533–5536. (b) Ashworth, I. W.; Hillier, I. H.; Nelson, D. J.; Percy, J. M.; Vincent, M. A. *Chem. Commun.* **2011**, *47*, 5428–5430. (c) Thiel, V.; Hendann, M.; Wannowius, K.-J.; Plenio, H. *J. Am. Chem. Soc.* **2012**, *134*, 1104–1114. (d) Nuñez-Zarur, F.; Solans-Monfort, X.; Rodríguez-Santiago, L.; Sodupe, M. *Organometallics* **2012**, *31*, 4203–4215. (e) Urbina-Blanco, C. A.; Poater, A.; Lebl, T.; Manzini, S.; Slawin, A. M. Z.; Cavallo, L.; Nolan, S. P. *J. Am. Chem. Soc.* **2013**, *135*, 7073–7079. (f) Manzini, S.; Urbina-Blanco, C. A.; Nelson, D. J.; Poater, A.; Lebl, T.; Meiries, S.; Slawin, A. M. Z.; Falivene, L.; Cavallo, L.; Nolan, S. P. *J. Organomet. Chem.* **2015**, *780*, 43–48.
33. Thorstenson, T.; Songstad, J. *Acta Chem. Scand.* **1976**, *30A*, 781–786.
34. (a) Zhao, Y.; Truhlar, D. G. *Org. Lett.* **2007**, *9*, 1967–1970. (b) Zhao, Y.; Truhlar, D. G. *Acc. Chem. Res.* **2008**, *41*, 157–167. (c) Minenkov, Y.; Occhipinti, G.; Jensen, V. R. *J. Phys. Chem. A.* **2009**, *113*, 11833–11844. (d) Zhao, Y.; Truhlar, D. G. *J. Chem. Theory Comput.* **2009**, 324–333. (e) Silwa, P.; Handzlik, J. *Chem. Phys. Lett.* **2010**, *493*, 273–278.
35. For a discussion and study of the structure of tris(dialkylamino)phosphines, see: Gonbeau, D.; Sanchez, M.; Pfister-Guillouzo, G. *Inorg. Chem.* **1981,** *20*, 1966–1973.
36. (a) Bowmaker, G. A.; Effendy; Skelton, B. W.; White, A. H. *J. Chem. Soc., Dalton Trans.* **1998**, 2123–2129. (b) Bowmaker, G. A.; Brown, C. L.; Hart, R. D.; Healey, P. C.; Rickard, C. E. F.; White, A. H. *J. Chem. Soc., Dalton Trans.* **1999**, 881–889.
37. Kroshefsky, R. D.; Verkade, J. G. *Inorg. Chem.* **1975,** *14*, 3090–3095.
38. Tolman, C. A. *Chem. Rev.* **1977**, *77*, 313–348.
39. Lin, T.-P.; Chang, A. B.; Chen, H.-Y.; Liberman-Martin, A. L.; Bates, C. M.; Voegtle, M. J.; Bauer, C. A.; Grubbs, R. H. *J. Am. Chem. Soc.* **2017,** *139*, 3896–3903.

For Table of Contents Only

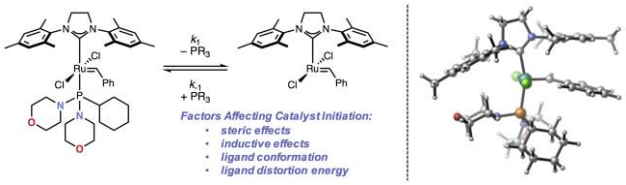

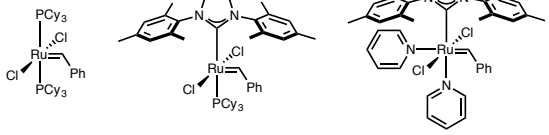

G1 **G2** **G3**

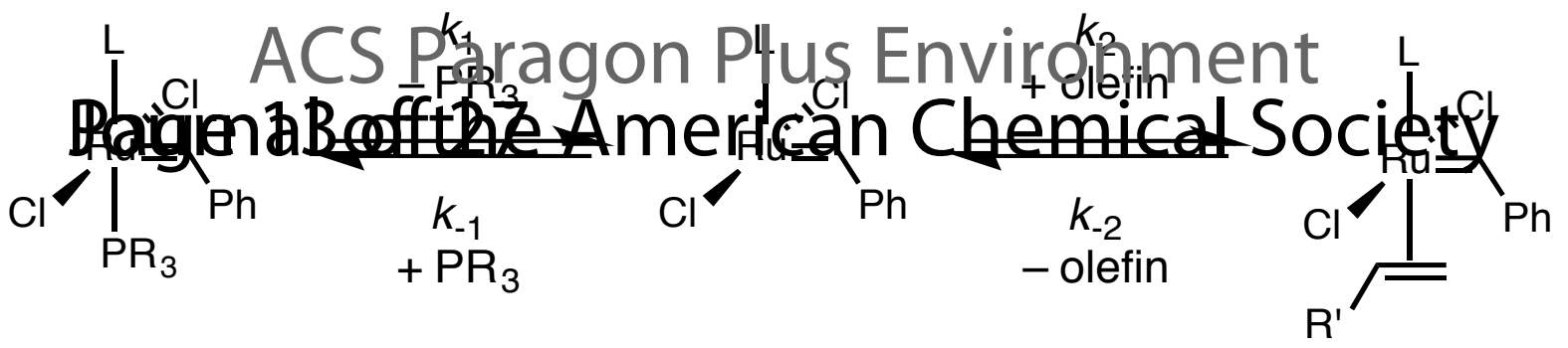

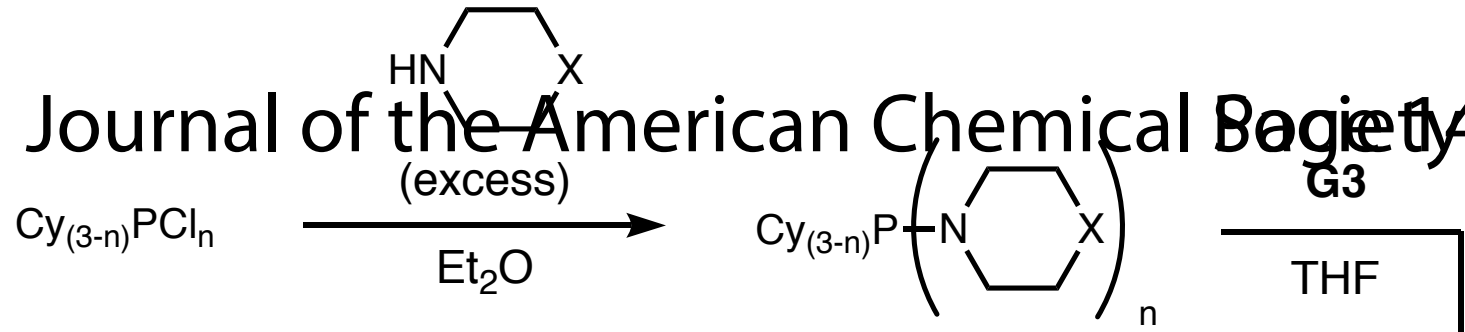

L1 (n = 1; X = O) **L4** (n = 1; X = CH_2)
L2 (n = 2; X = O) **L5** (n = 2; X = CH_2)
L3 (n = 3; X = O) **L6** (n = 3; X = CH_2)

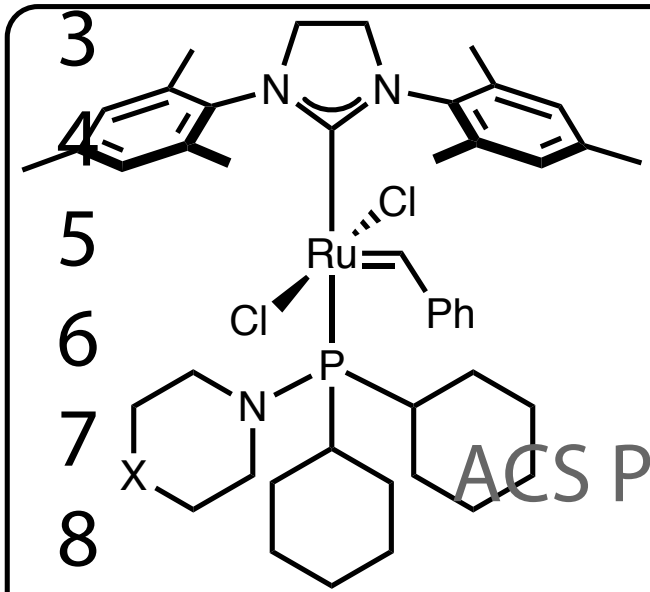

1 (X = O)
4 (X = CH_2)

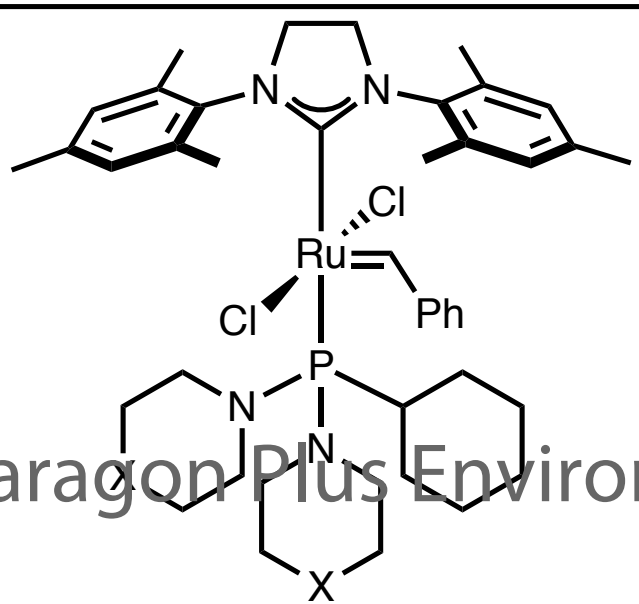

2 (X = O)
5 (X = CH_2)

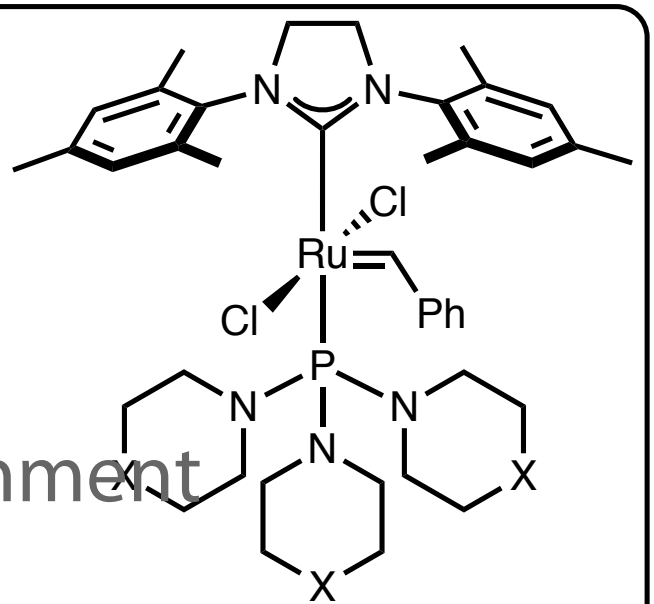

3 (X = O)
6 (X = CH_2)

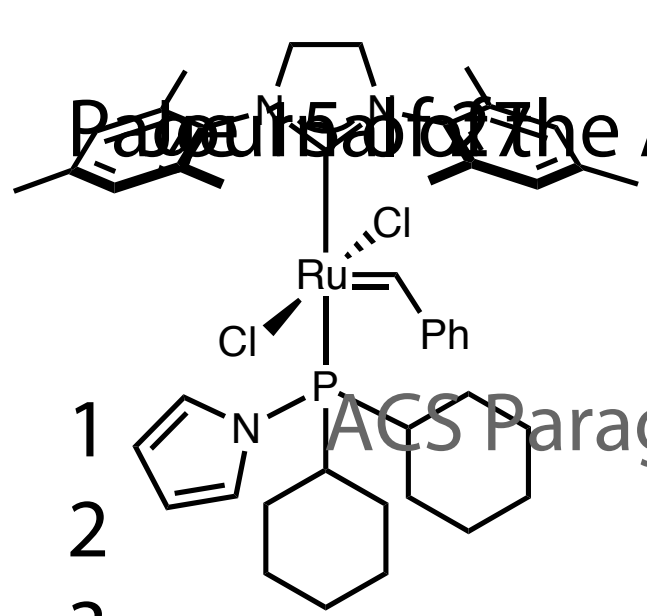

7

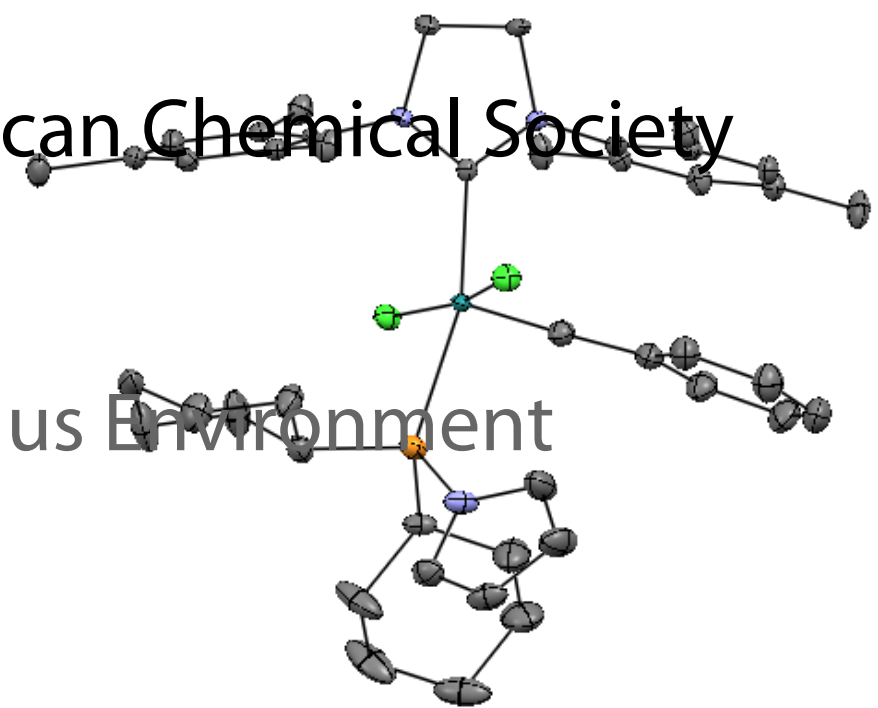

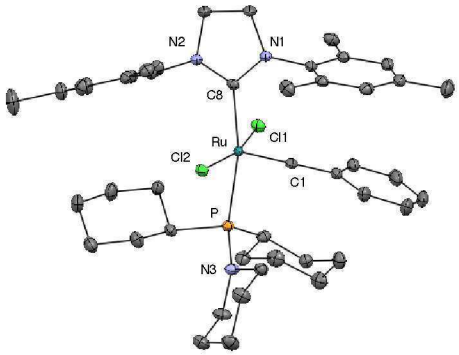
N2
N1
C8
Ru
Cl1
Cl2
C1
P
N3

Journal of the American Chemical Society

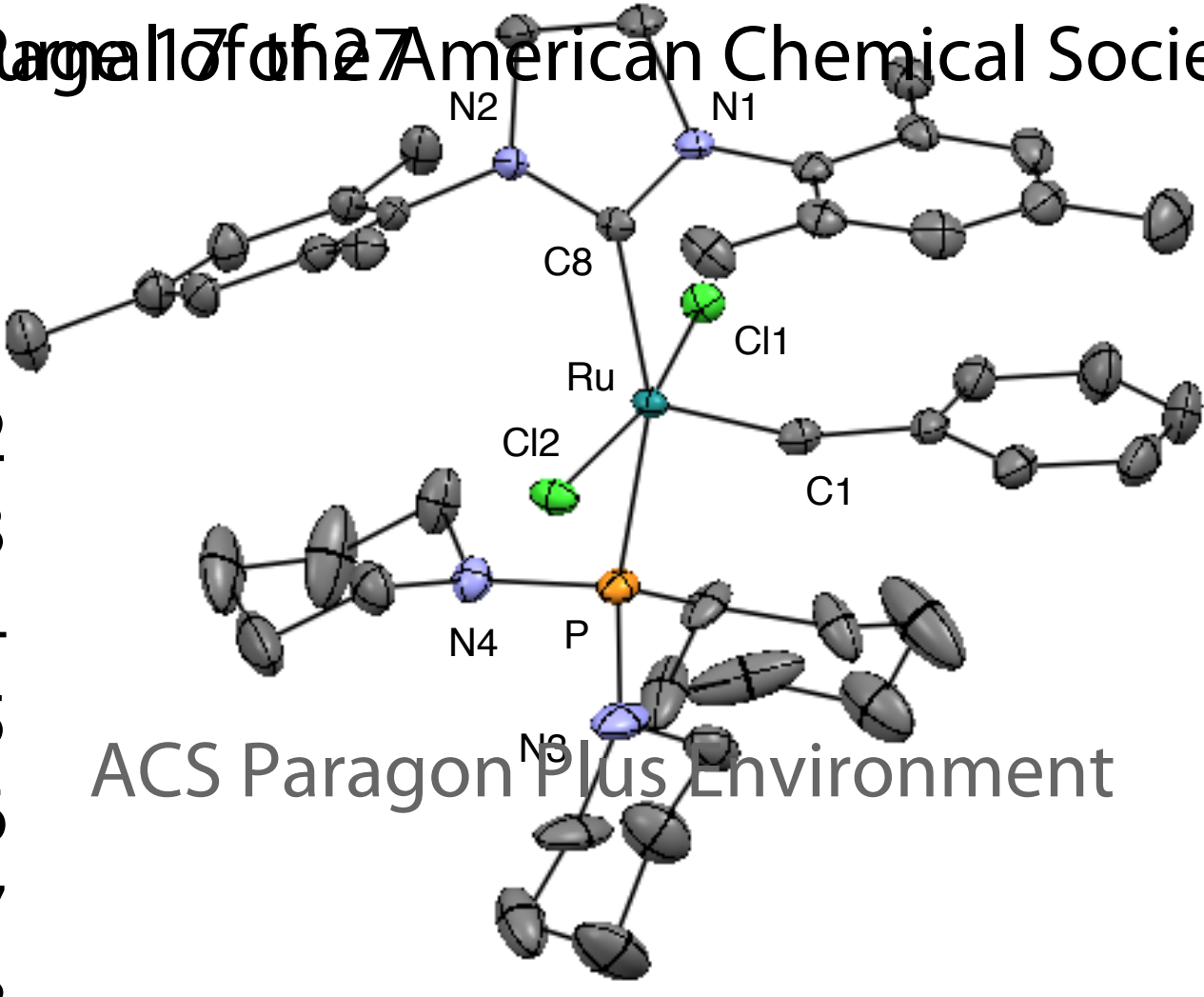

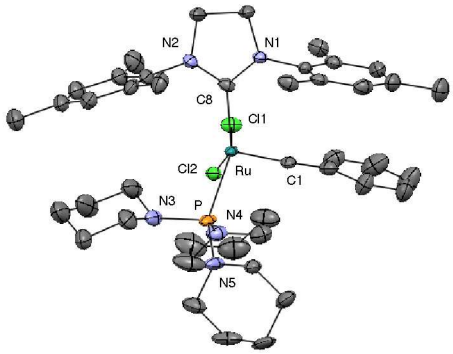
N2
N1
C8
Cl1
Cl2
Ru
C1
N3
P
N4
N5

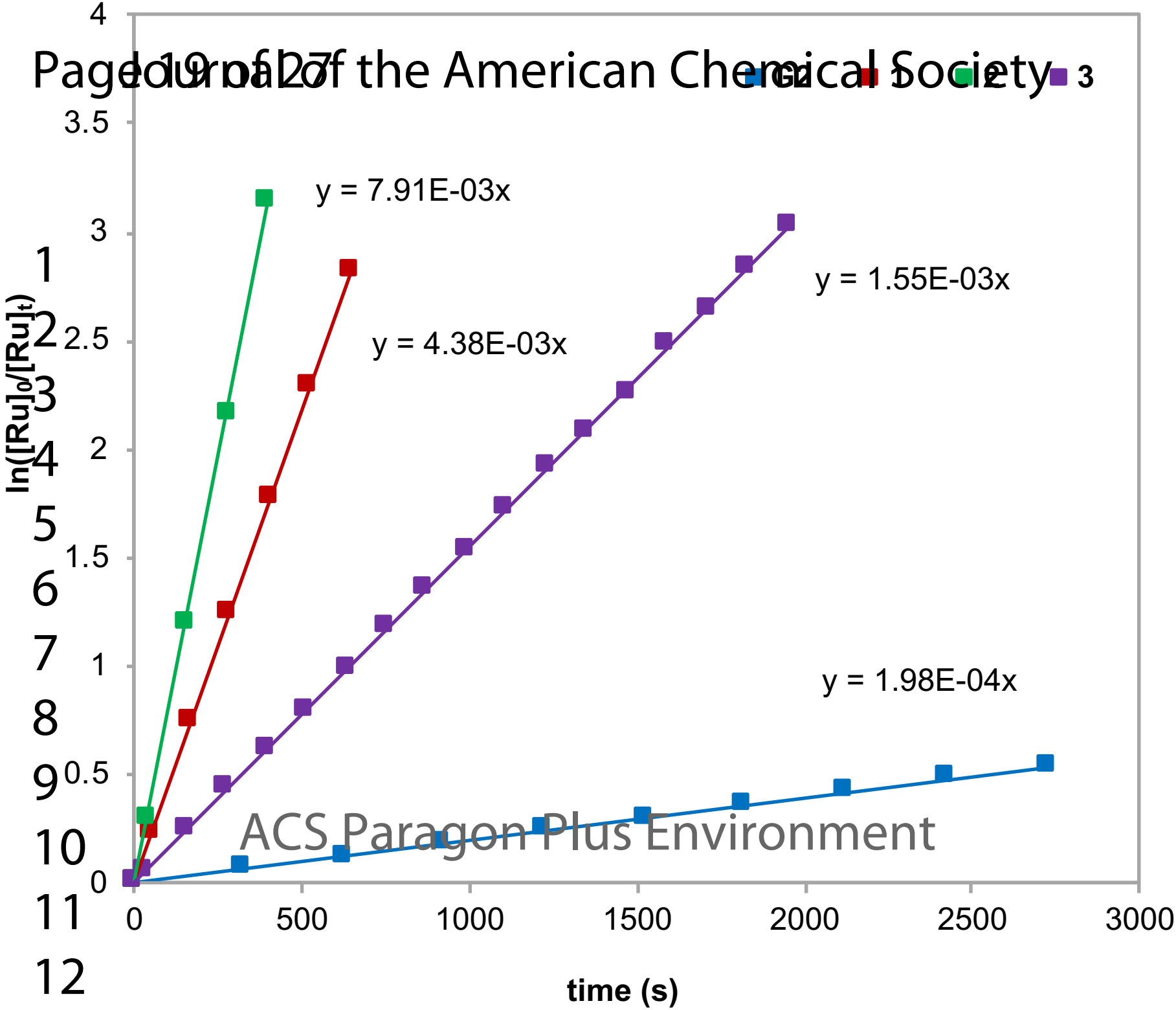
4
3.5
3
2.5
2
1.5
1
0.5
0
0
500
1000
1500
2000
2500
3000
time (s)
ln([Ru]0/[Ru]t)
y = 7.91E-03x
y = 4.38E-03x
y = 1.55E-03x
y = 1.98E-04x
1
2
3
ACS Paragon Plus Environment

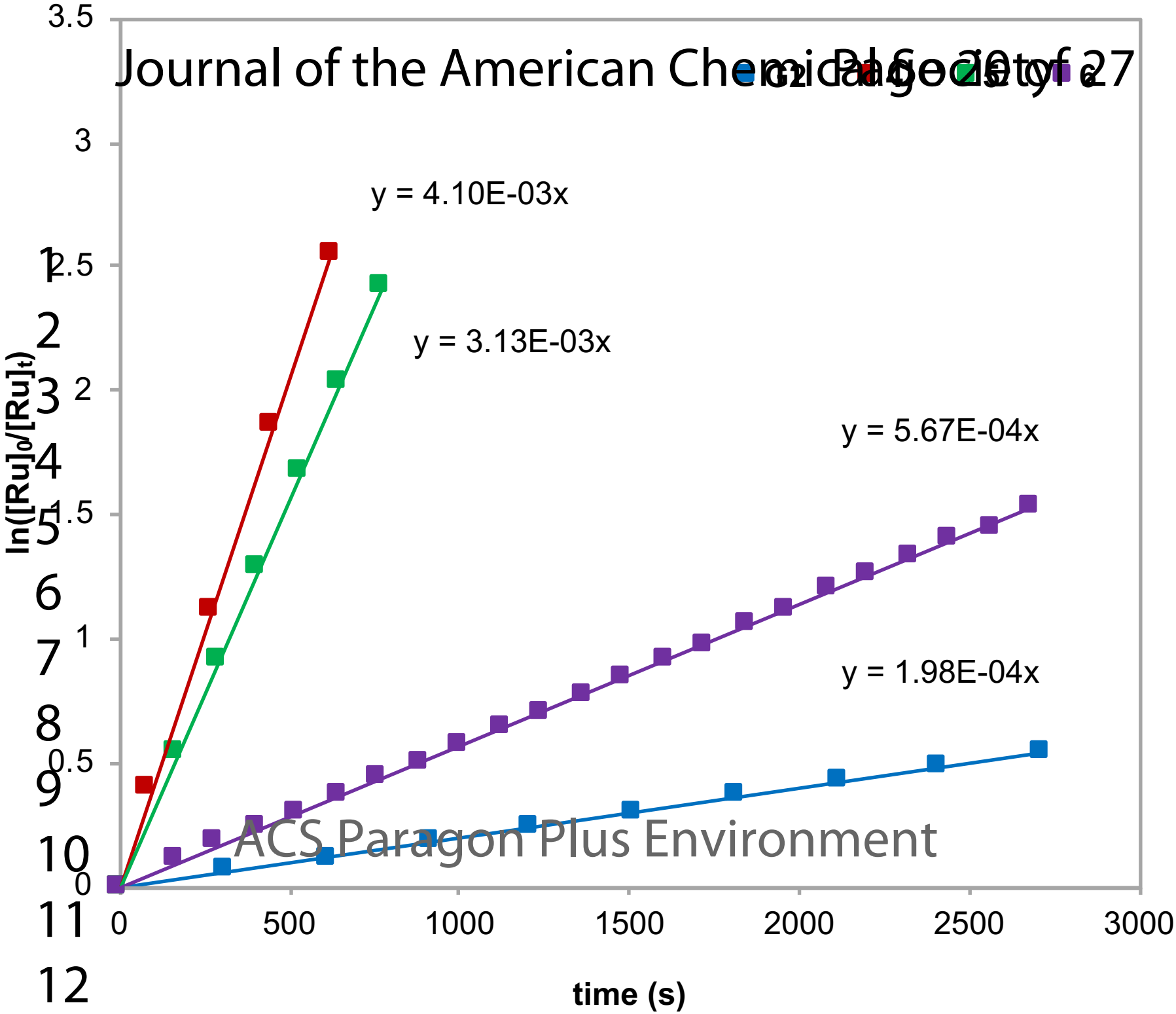

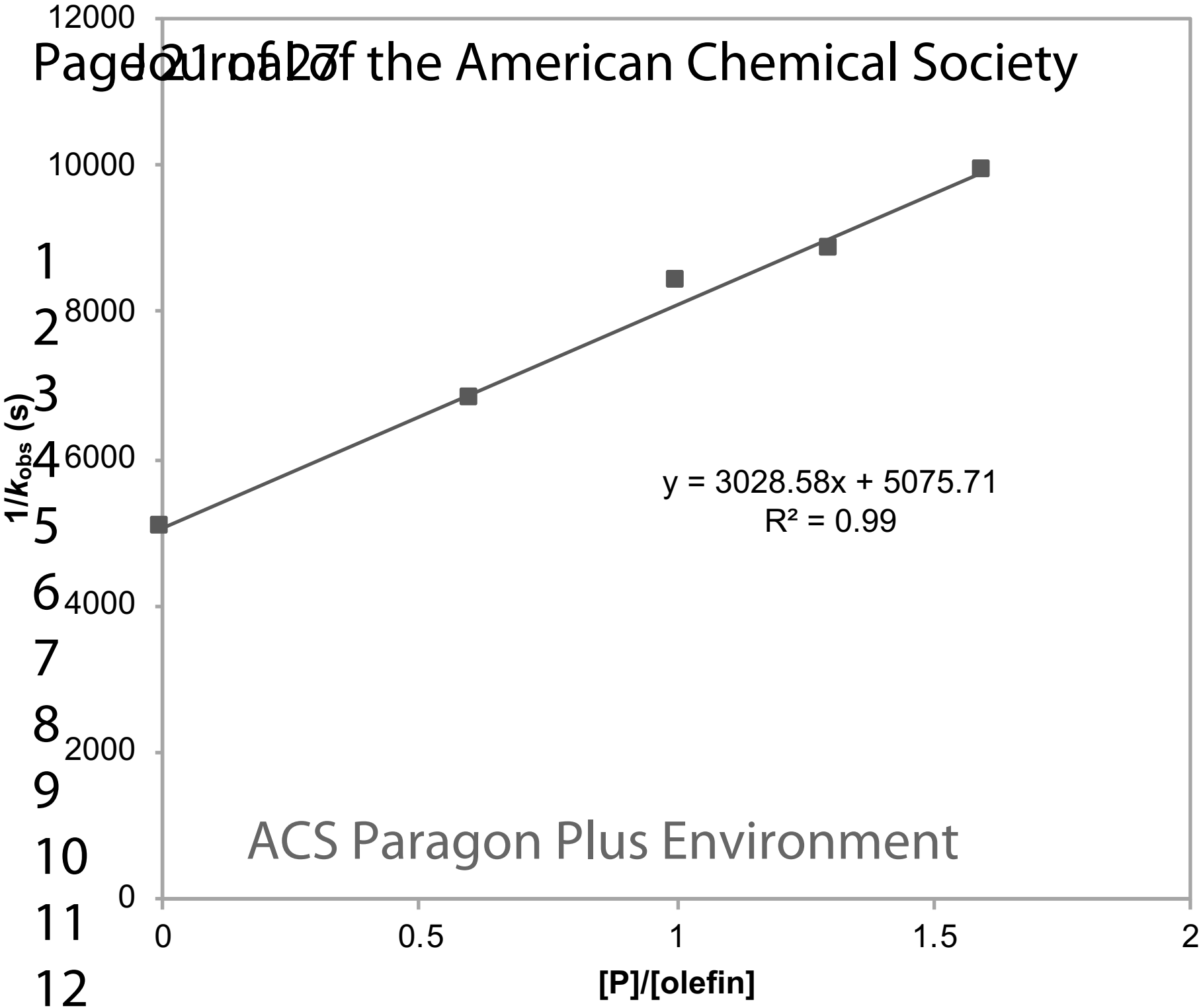
12000
10000
8000
6000
4000
2000
0
1/kobs (s)
y = 3028.58x + 5075.71
R² = 0.99
0
0.5
1
1.5
2
[P]/[olefin]
ACS Paragon Plus Environment

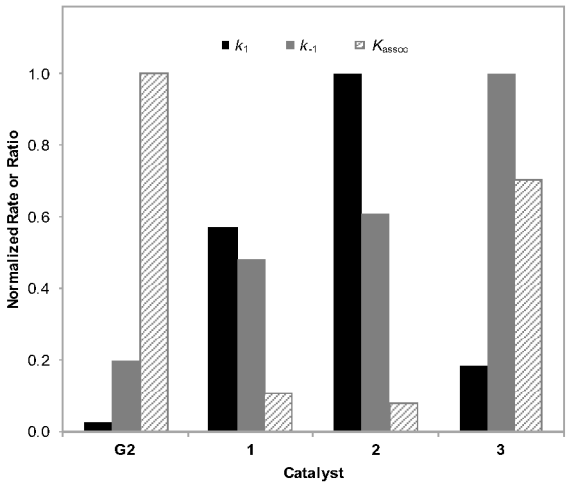
k_1
k_{-1}
K_{assoc}
1.0
0.8
0.6
0.4
0.2
0.0
Normalized Rate or Ratio
G2
1
2
3
Catalyst

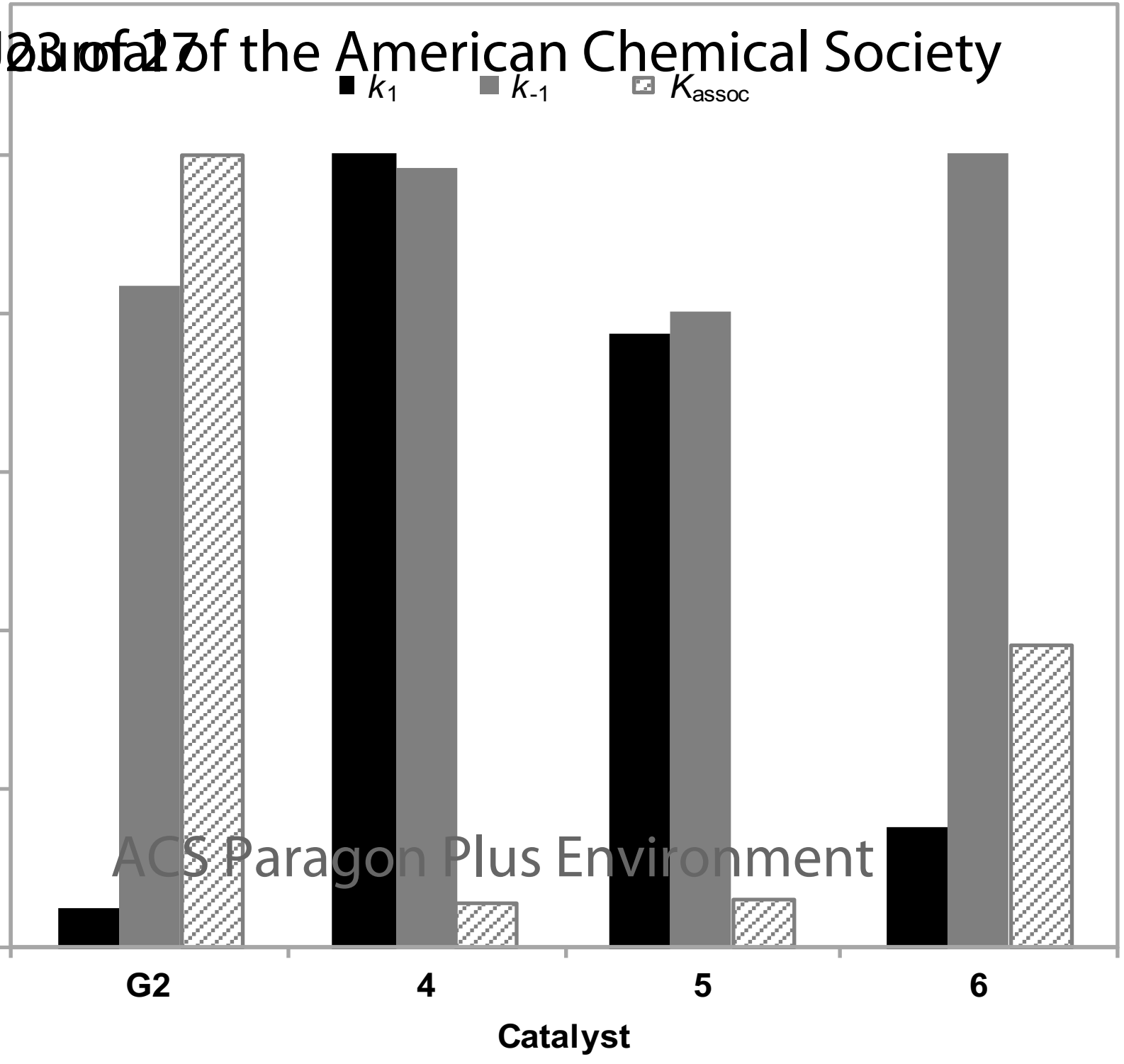

Simplified Representation *(Top-Down View)*

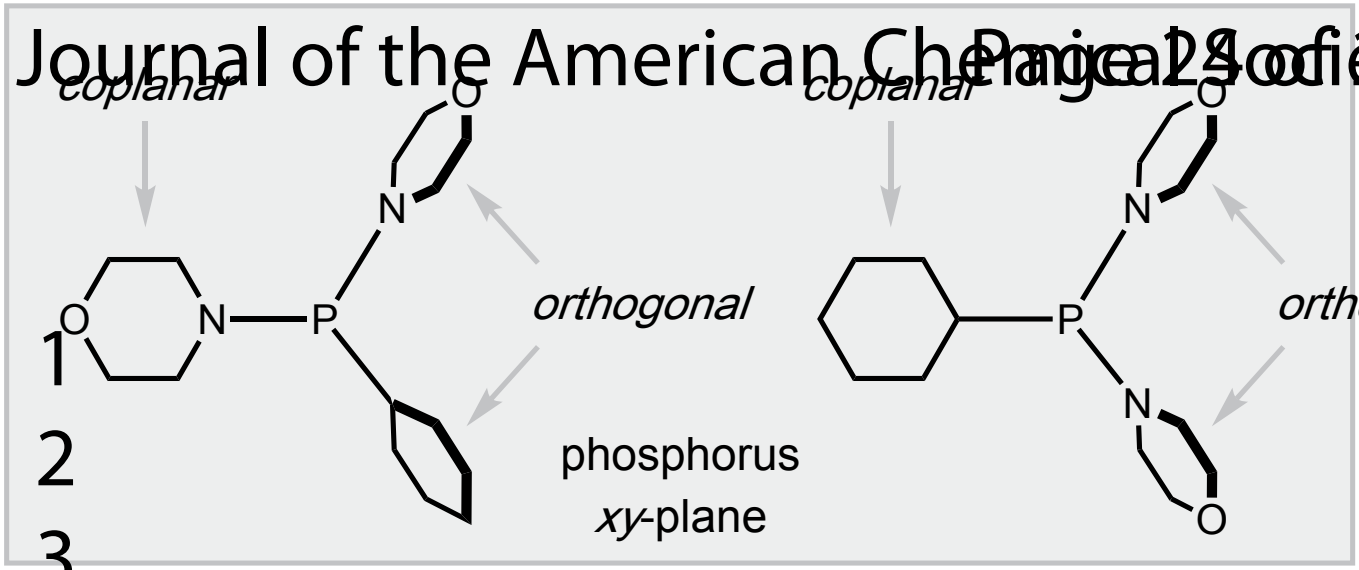

L2 (A) **L2 (B)**

DFT-Calculated Conformations *(Side-On View)*

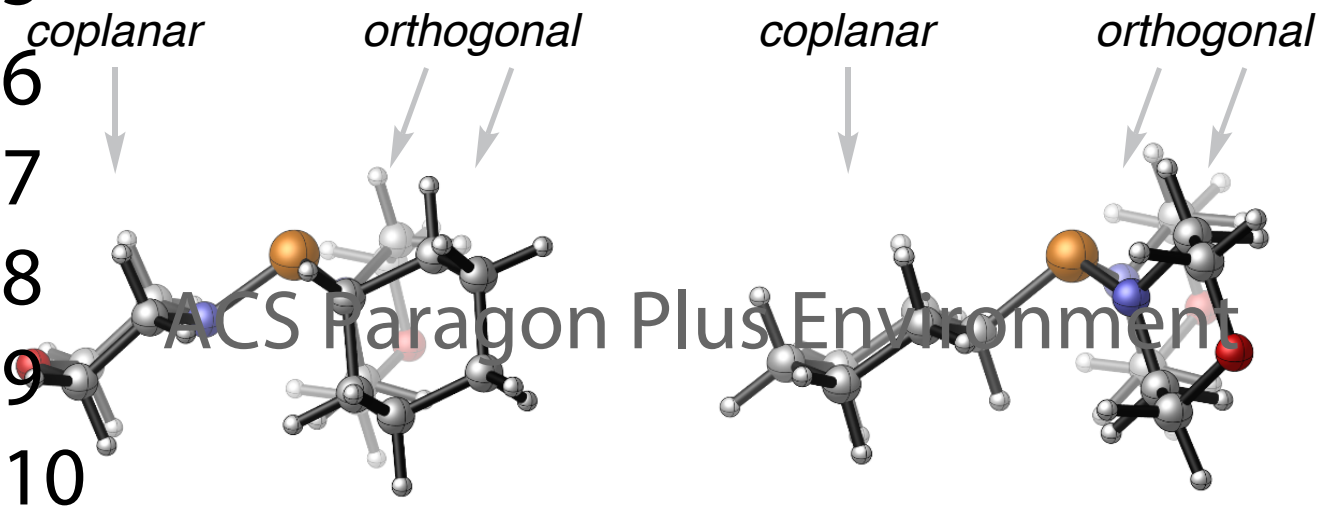

L2 (A) $\Delta G = -4.0$ kcal/mol **L2 (B)**

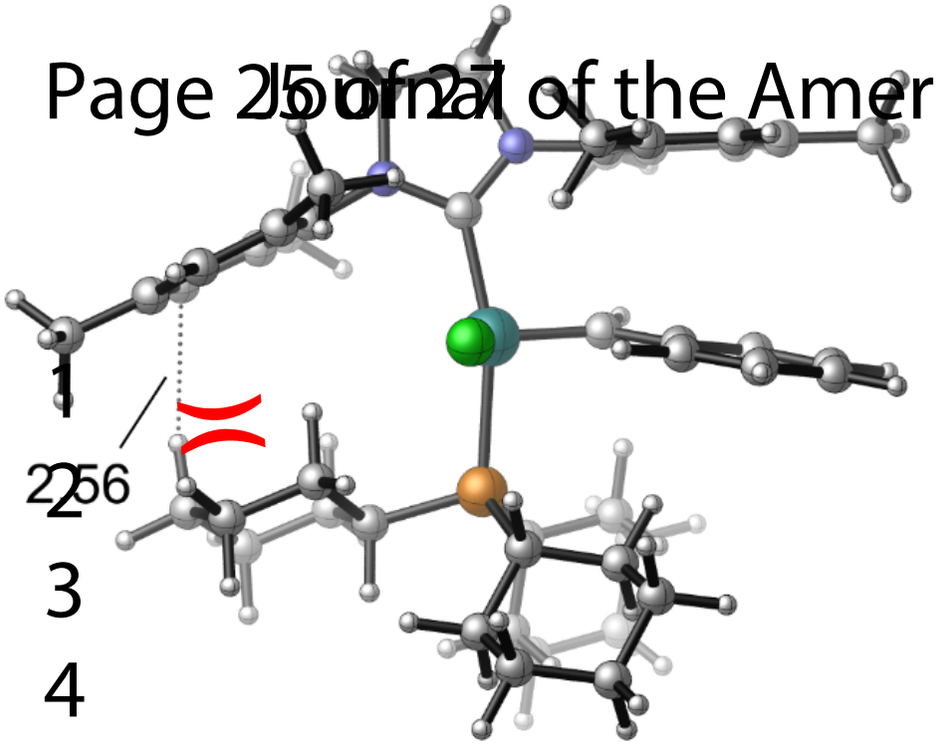

G2

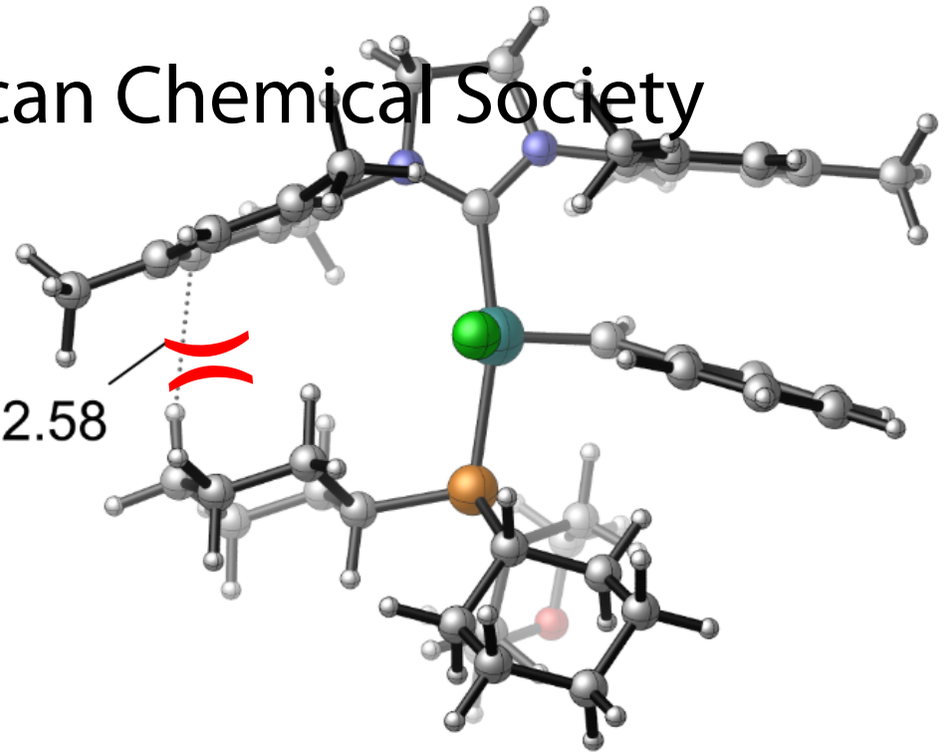

1

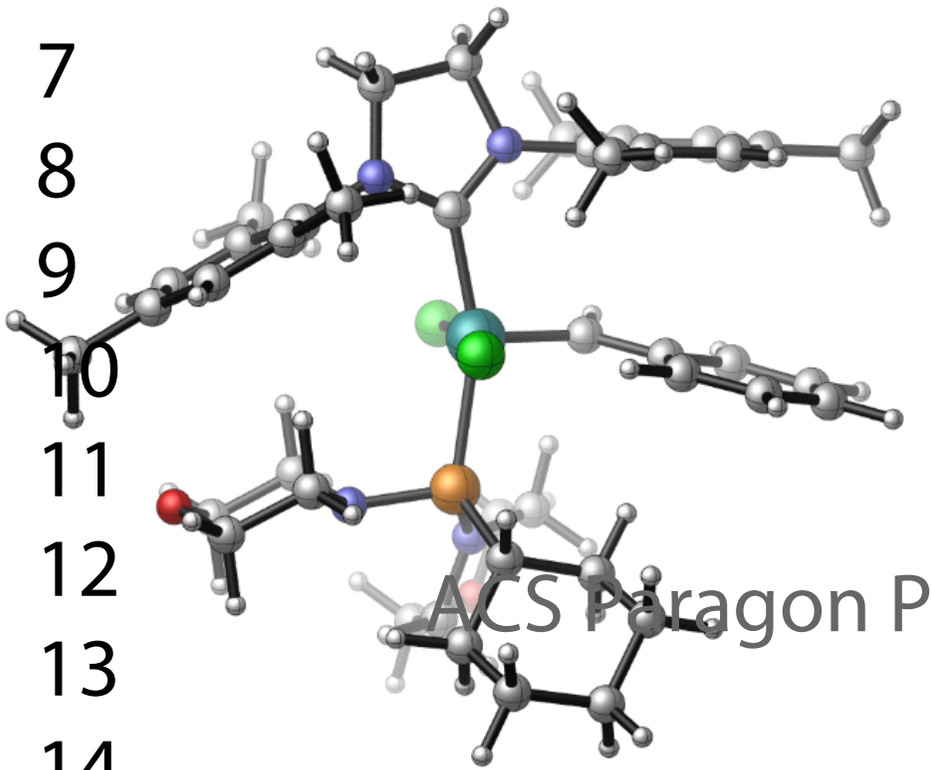

2

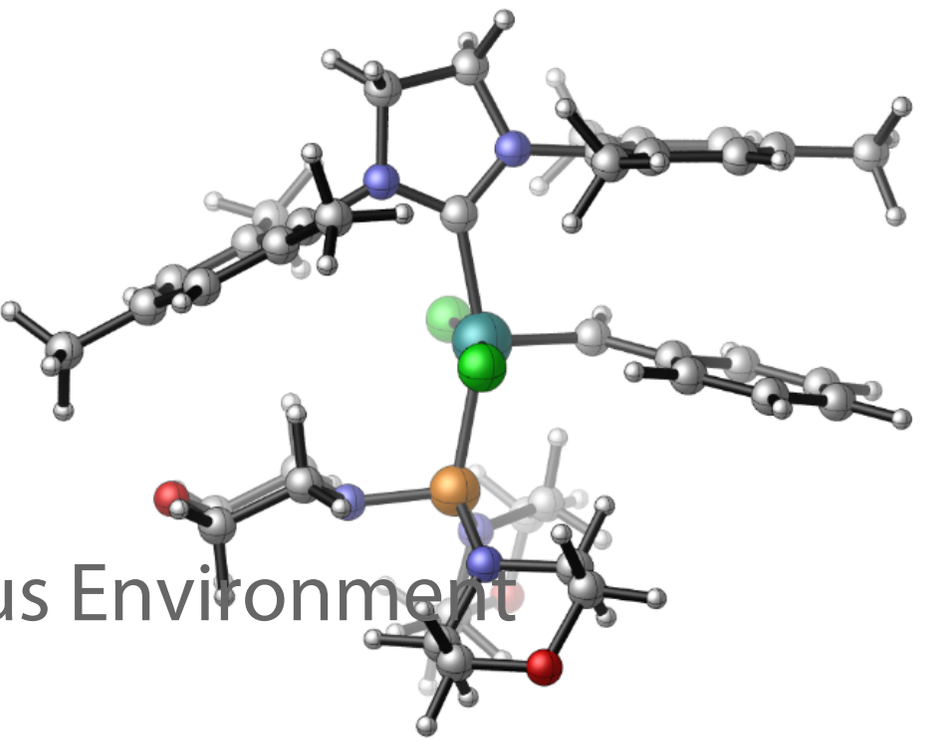

3

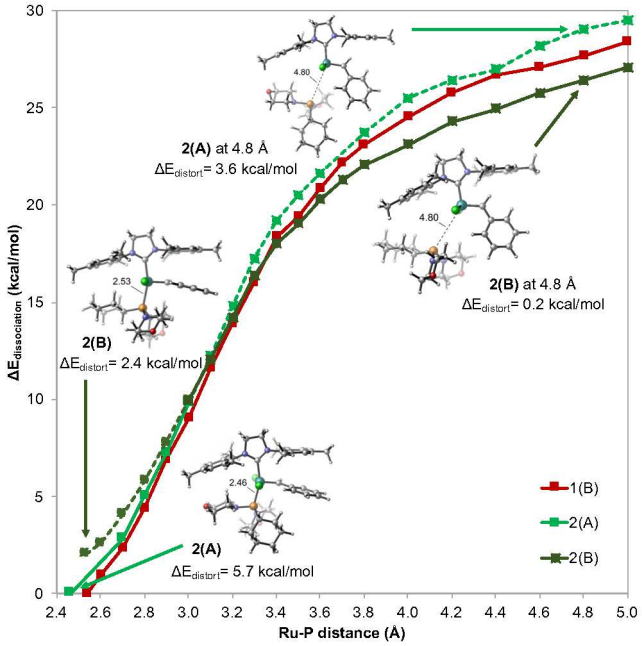
30
25
20
15
10
5
0
2.4
2.6
2.8
3.0
3.2
3.4
3.6
3.8
4.0
4.2
4.4
4.6
4.8
5.0
ΔE dissociation (kcal/mol)
Ru-P distance (Å)
2(A) at 4.8 Å
ΔE distort = 3.6 kcal/mol
2(B) at 4.8 Å
ΔE distort = 0.2 kcal/mol
2(B)
ΔE distort = 2.4 kcal/mol
2(A)
ΔE distort = 5.7 kcal/mol
4.80
4.80
2.53
2.46
1(B)
2(A)
2(B)

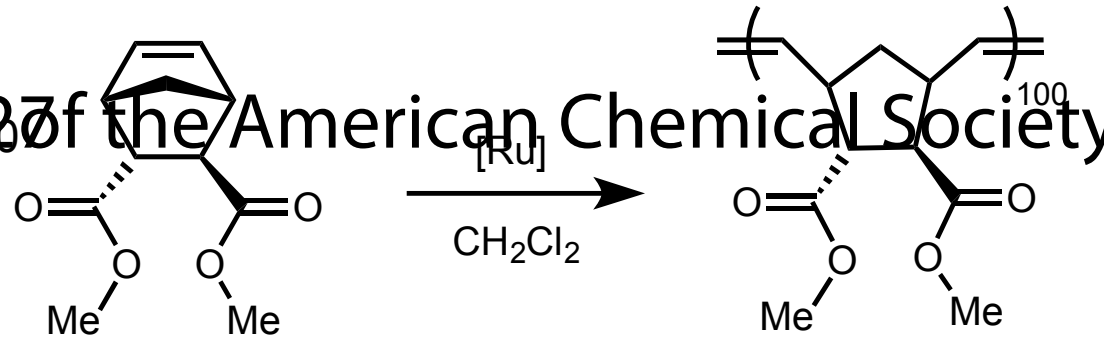
[Ru]
CH_2Cl_2
Me
Me
Me
Me

8 **9**

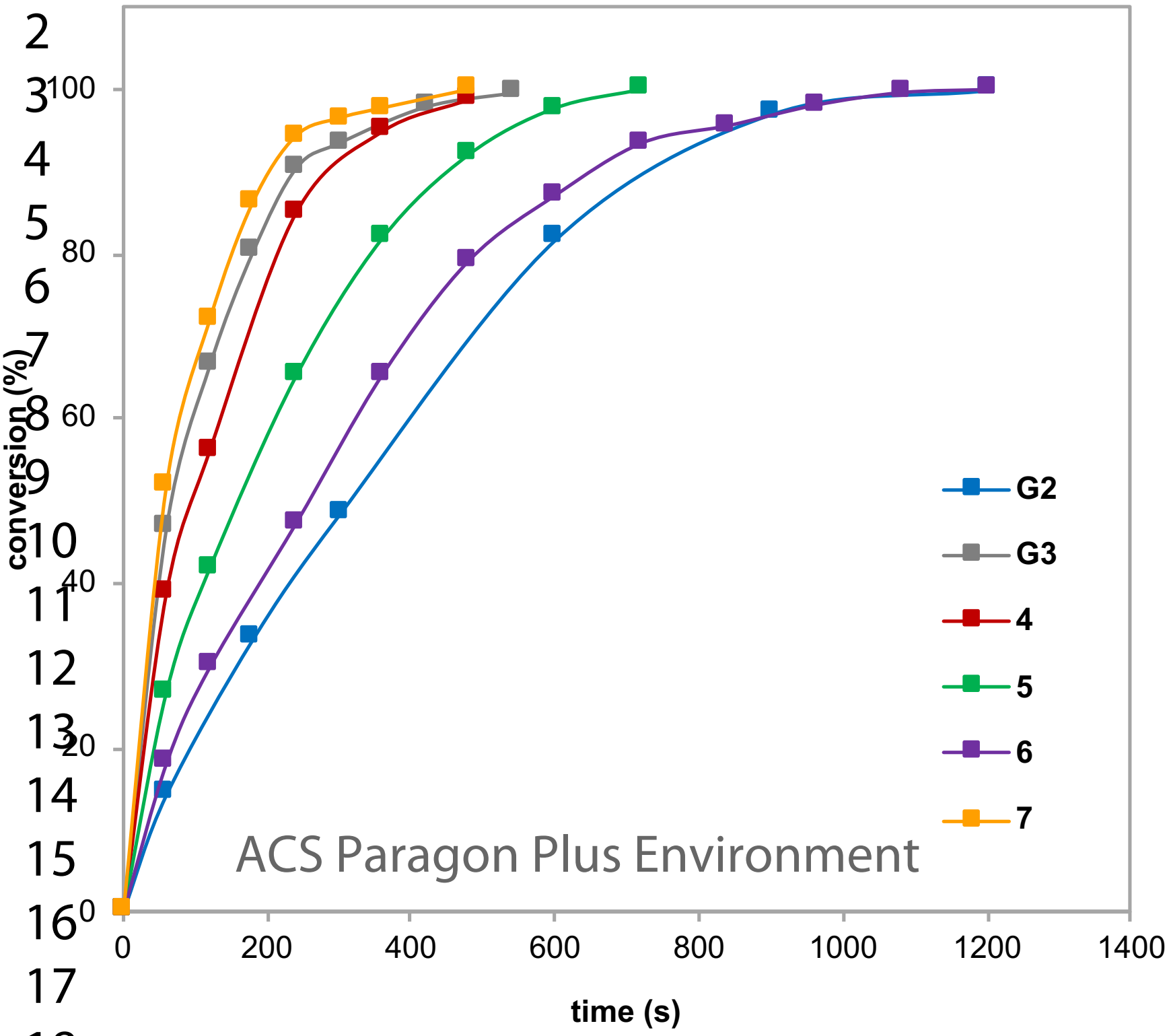
conversion (%)
time (s)
0
20
40
60
80
100
0
200
400
600
800
1000
1200
1400
G2
G3
4
5
6
7
ACS Paragon Plus Environment